ASTRONOMY & ASTROPHYSICS
SUPPLEMENT SERIES

DECEMBER **1987**, PAGE 603

Astron. Astrophys. Suppl. Ser. **71**, 603-642 (1987)

0.6 GHz mapping of extended radio galaxies. III. 3C66B, NGC 1265, 3C129, DA240, 3C236, 4C48.29, IC708 & IC711, 4CT51.29.1, 3C310, Abell2256, 3C402 and 3C465

W. J. Jägers

Sterrewacht Leiden, Postbus 9513, 2300 RA Leiden, The Netherlands

Received June 15, accepted July 27, 1987

Summary. — Radio observations made with the Westerbork Telescope at 0.6 GHz are presented for 12 extended radio sources : 3C66B, NGC 1265, 3C129, DA240, 3C236, 4C48.29, IC708 & IC711, 4CT51.29.1, 3C310, Abell2256, 3C402 and 3C465. Previously observed Westerbork data at 1.4 GHz are convolved for comparison with the 0.6 GHz data. In addition maps of the total intensity and linear polarization structure, the distributions of the spectral index, the depolarization and the rotation of the polarization position angle between 0.6 GHz and 1.4 GHz have been derived. Integrated values for the total intensity and the polarization are also given.

Key words : active galaxies — radio galaxies — polarization — radio sources.

1. Introduction.

This is the third of a series of papers describing the 0.6 GHz observations made with the 3 km Westerbork Synthesis Radio Telescope (WSRT) of a sample of 30 extended extragalactic radio sources. In addition convolved 1.4 GHz observations made in previous studies with the 1.5 km WSRT are included for comparison of the resultant maps at both frequencies.

Taken as a whole the sample is representative of the various morphological types found among radio galaxies (e.g. Miley, 1980). It is limited to radio sources larger than 200 arcsec and those with declinations above 25°. The two preceding papers describe the observations of 9 edge-brightened double sources (Jägers, 1987 : Paper I) and of 8 edge-darkened double sources (Jägers, 1987a, Paper II) respectively. The radio source 0945+734 (4C73.08) will be discussed separately because, in addition to the observations at 0.6 GHz and 1.4 GHz, observations at 327 MHz, also made with the WSRT, will be available. This makes a three frequency comparison with a reasonable resolution possible.

The observations of the remaining 12 radio sources are described in this paper : 0219+427 (3C66B), 0314+416 (NGC 1265), 0445+449 (3C129), 0744+559 (DA240), 1003+351 (3C236), 1017+497 (4C48.29), 1131+492 (IC708 & IC711), 1200+519 (4CT51.29.1), 1502+262 (3C310), 1706+787 (Abell2256), 1940+504 (3C402) and 2335+267 (3C465).

1.1 Observations and data reduction.

The 12 radio sources were observed with the 3 km WSRT at a frequency of 608.5 MHz. The calibration and reduction of the observational data were described in detail in Paper I.

The parameters of the present 0.6 GHz observations are listed in table I.

Column 1 : the source name.

Column 2 : an alternative source name.

Columns 3, 4 : the centre of the observed field in equatorial coordinates (1950.0). The diameter of the primary beam at 0.6 GHz is 1.4 degrees.

Columns 5 ; 6 : the centre of the observed field in galactic coordinates.

Column 7 : the date of observation. Every line represents an observation of 1×12 h.

Column 8 : the receivers used. The frequency of the observations is 608.5 MHz with a bandwidth of 2.5 MHz. The sensitivity of the receivers was improved at the end of 1981.

The « old » receivers had a system noise temperature of about 350 K compared with a system noise temperature of about 100 K for the « new » receivers.

Columns 9, 10, 11 : the interferometer configuration giving the : shortest baseline — increment — longest baseline for the 1 or 2×12 h observation.

Column 12 : the half power width of the synthesized beam.

Columns 13, 14 : the RMS noise and the confusion level in the total intensity map.

One of the reasons for observing the radio sources at 0.6 GHz was to make a comparison with 1.4 GHz data. For 9 of the 12 source satisfactory 1.4 GHz observations with the 1.5 km WSRT were available. NGC 1265 was reobserved in 1982 with the 3 km WSRT. The 1.4 GHz observational data of DA240 and 3C236 were not suitable for comparison with the 0.6 GHz data. Relevant parameters of the 1.4 GHz observations are listed in table II.

Column 1 : the source name.

Column 2 : an alternative source name.

Columns 3, 4 : the exact frequency and bandwidth of the 1.4 GHz observation.

Column 5 : the year of observation.

Columns 6, 7 : the RMS noise and the confusion level in the total intensity maps, determined from the convolved maps.

Column 8 : notes giving the references for the 1.4 GHz full resolution maps. See the notes to table II.

To make a satisfactory comparison between the intensity maps at the two different frequencies as described in Paper I, the 1.4 GHz observations were reduced again to obtain an effective resolution equal to that of the 0.6 GHz observations. The *UV* coverages (in wavelengths) at both frequencies were made as much as possible the same. The maps were restored, after cleaning, with similar Gaussian beam.

The resulting maps were used to compare the intensity distributions at both frequencies.

1.2 RESULTS. — Figures 1 to 12 present the results.

In each case panel « a » shows a contour plot of the total intensity distribution of the radio source at 0.6 GHz. The dashed contours represent « negative » brightness values. Superimposed on each map are the position angles of the electric vector of the linearly polarized intensity with arbitrary lengths. The ellipse represents the half power intensity of the synthesized beam. A cross marks the position of the optical galaxy identified with each radio source. Panel « b » shows a contour plot of the linearly polarized intensity distribution at 0.6 GHz superimposed on a two-level gray scale plot of the total intensity distribution. Figure « c » shows a gray scale plot of the distribution of the percentage polarization at 0.6 GHz superimposed on a two-contours plot of the total intensity distribution. Note that for the percentages polarization the first gray values represent upper limits i.e. they indicate regions where the percentage polarization is smaller than the indicated value. Higher levels represent absolute values.

Panels « d », « e » and « f » show the some quantities as « a », « b » and « c » at 1.4 GHz, i.e. the total intensity distributions, the intensity of the linear polarization, and the percentage polarization.

Panels « g », « h » and « i » show the distributions of the spectral index, the depolarization and the rotation of the electric vector superimposed on two-level plots of the total intensity distribution at 0.6 GHz.

Panel « j » is a plot of spectral index variations along the radio source. The lower panel shows the integrated total intensity (parallel to the minor axis) along the major axis of the radio source at 0.6 GHz (thick line) and 1.4 GHz (thin line). The two lines have been normalized to the maximum of the 0.6 GHz curve. The upper panel shows the spectral index variations. Values with uncertainties larger than 1.0 are omitted. 0 marks the position of the optical galaxy. The points in the curves are not independent as they reflect values with a separation of one grid-point. In general each independent beam comprises 2.8 points in both dimensions.

Table III lists integrated values for the total intensity, the percentage linear polarization and the position angle of the electric vector at 0.6 GHz and 1.4 GHz for each source. The integrated values have been determined by summing the pixel intensities in appropriate parts of the maps and dividing by the volume in the synthesized beam. This was done for the I, Q and U-maps. The values for the integrated percentages of polarization and the polarization position angles have been calculated using the integrated I, Q and U values.

The uncertainties in the various quantities have been determined using the rms noise levels and confusion levels as given in tables I and III. As mentioned previously the integrated percentage polarization can be small although there is locally significant polarization. The uncertainty can therefore be larger than the value itself. In these cases an upper limit has given which is the sum of the value and its uncertainty. The corresponding position angles are then enclosed in between brackets.

2. Notes on individual sources.

3C66B. — 3C66B has one of the most peculiar forms in the 3C catalogue (Miley and Van der Laan, 1973). However, its rather complicated morphology has features in common with 3C31 (Van Breugel, 1982).

Northover (1973) and Van Breugel and Jägers (1982) showed at 5.0 GHz that the overall appearance of 3C66B resembles that of a trumpet fed by an expanding jet which appears to open abruptly, at one end. The jet has an optical counter jet (Butcher *et al.*, 1980). 3C66B also has a weak radio counter jet. At 1.4 GHz its overall appearance is that of a head-tail source seen partly head- or tail-on. It has been suggested that 3C66B has an appreciable velocity component eastwards (Van Breugel, 1982). The morphology may haven been further complicated by orbital motion because there are two nearby companion galaxies (Butcher *et al.*, 1980).

Near the base of the jet the projected magnetic field flips from parallel to perpendicular (Van Breugel, 1982). At its centre it remains perpendicular all the way to the end of the widening jet but along the sides it is parallel in some places. Also in the lobes the magnetic field is parallel to the boundaries. A five-frequency comparison of 366B has been made by Leahy *et al.* (1986).

The 3 km WSRT observations of 3C66B at 0.6 GHz show a polarization structure that follows the ridge of stronger emission in the total intensity distribution. This detailed structure coincides roughly with that at 1.4 GHz, although the intensity (as well as the fractional polarization) is smaller. The polarization position angle rotates along the ridge.

The rotation of the polarization position angle between 0.6 GHz and 1.4 GHz can be divided into several separate regions in the radio source. At these regions where emission at 5.0 GHz is visible (Van Breugel and Jägers, 1982) the spectrum is relatively flat ; in the surrounding regions the spectrum is much steeper.

NGC1265. — The head tail radio source NGC 1265 has been the subject of many investigations (e.g. Miley *et al.*, 1975 ; Owen *et al.*, 1978 ; Gisler and Miley, 1979).

Miley *et al.* (1975) presented 1.5 km WSRT data at 5.0 GHz and compared it with older 1.4 GHz WSRT data (Miley, 1973). They showed that the magnetic field vectors are well aligned along the tail and from the high percentage polarization in several places concluded that the magnetic energy is dominant. In addition there appears to be a rotation measure gradient across the tail. The 5.0 GHz data show a nuclear radio component and two parallel radio jets extending to the North. The results are in agreement with the predictions of the magnetospheric trail model for head tail sources (Jaffe and Perola, 1973).

High resolution Very Large Array (VLA) maps at 4.9 GHz (Owen *et al.*, 1978) show two narrow wobbly continuous streams of emission leading away from the nucleus out into the lower-surface brightness tail. Both jets, which have several knots of emission are not visibly connected to the nucleus.

Gisler and Miley (1979) showed the existence of a large low brightness emission extension toward the North-East together with a small extension toward the South-West. They suggested that the weak extension to the North-East is a dense tail which traces the actual orbit of NGC 1265 while the main body of the tail has been bent away from the cluster center by buoyancy forces.

The full resolution 0.6 GHz observation of NGC 1265 made with the 3 km WSRT shows no evidence for the existence of the weak extension to the North-East. However the maps which have been convolved to a beam of 1 arcmin confirm its existence. The spectral index continuously increases along the tail but compared with the other head-tail sources discussed in this paper, such as 3C129 and IC711 the spectrum remains relatively flat.

At 0.6 GHz there is only weak polarization in NGC 1265, mainly at the region of the head. This means that the depolarization between 0.6 GHz and 1.4 GHz is large.

3C129. — 3C129 is the prototype narrow tailed galaxy. This radio source has been studied by many authors (e.g. Miley, 1973 ; Rudnick and Burns, 1981). Van Breugel and Jägers (1982) presented 1.5 km WSRT observations of 3C129 at 0.6 GHz and 5.0 GHz. At 5.0 GHz, two parallel jets are visible with equivalent wiggles departing from the radio core. Icke (1981) showed that the radio trail of 3C129 can be reproduced by a model in which plasma beams precess as the galaxy traverses the intergalactic medium. At 0.6 GHz a head-tail structure is visible in which the tail is about 30 arcmin long.

Van Breugel (1982) deduced the magnetic field direction along the radio source. At the beginning of the jets the field is predominantly parallel to the major axis. As the jets expand, the field changes to a direction perpendicular to the jets and follows a behaviour similar to that observed in 3C31 and 3C66B. Further from the head and along the entire tail, the field is parallel to the source axis with only locally slight twists. The parent galaxy of 3C129 is a member of a poor cluster, which also includes 3C129.1, east of 3C129, a smaller double radio source which may also be tailed (Miley *et al.*, 1972 ; Downes, 1980).

The 3 km WSRT observations of 3C129 at 0.6 GHz show a previously unknown feature on the northeastern side of the head of 3C129 (Jägers and De Grijp, 1983). It is proposed that this steep spectrum component is a relic of enhanced activity in the nucleus of 3C129 some 10^7 yr ago.

There is high depolarization between 0.6 GHz and 1.4 GHz. Only a few polarization peaks are visible in the 0.6 GHz map. In the tail a weak double polarization structure is visible comparable with that in the edge-darkened double resources 3C130 and 3C449.

The spectral index between 0.6 GHz and 1.4 GHz increases intermittently along the tail from the head, as had been previously indicated by Van Breugel (1982).

3C129.1 is barely polarized at 0.6 GHz. The run of spectral index along 3C129.1 is that of a narrow edge-darkened double radio source (Paper II).

3C236. — 3C236 is the largest known radio source, with a total linear size of ~ 4 Mpc ($z = 0.0988$, $H_0 = 75$ km s^{-1} Mpc^{-1}). Not only the extended structure has been studied in great detail (e.g. Strom and Willis, 1980 ; Strom *et al.*, 1981) but also its strong radio core (e.g. Folamont *et al.*, 1982 ; Barthel *et al.*, 1984).

Low resolution observations show a large narrow double structure including a steep spectrum core. The spectral index distribution between 0.6 GHz and 4.8 GHz (Strom *et al.*, 1981) shows that in the western lobe the spectrum steadily steepens from the leading edge towards the centre. There is weak evidence that in the eastern lobe, the spectrum of the tail is steeper than that of the head. 3C236 possesses a high degree of polarization with only slight depolarization between 1.4 GHz and 0.6 GHz while the rotation measure within each component is nearly constant. The magnetic field is quite uniform, generally runs parallel to contours in the total intensity distribution and has a high degree of order (Strom and Willis, 1980).

Striking similarities between the large and small scale structure are found (Barthel *et al.*, 1984). Assuming a physical origin for these similarities it has been argued that long-lasting asymmetric behaviour of the inefficient energy flow interacting with galactic material is responsible for the overall morphology in 3C236. The flow of energy from the galactic nucleus may be continuous on one side and « blobby » on the other (Folamont *et al.*, 1982).

The 3 km WSRT observations of 3C236 at 0.6 GHz confirm the high degree of polarization. Both lobes show an appreciable amount of detail in the polarization distribution. The percentage polarization can rise up to ~ 20 %. In the western lobe this occurs mainly along the southern edge, in the eastern lobe it is seen throughout the component.

In the western component the polarization position angle is mainly perpendicular to the major axis except for the part closest to the radio core where it is roughly parallel. In the eastern component it is almost everywhere parallel to the source axis except for the outer edge where it is perpendicular.

DA240. — Strom *et al.* (1981) presented radio maps of DA240 made with the 1.5 km WSRT at 0.6 GHz and with the Effelsberg Telescope at 4.8 Ghz. They showed that the relative width of both lobes appears to decrease with increasing frequency, the (four) bright peaks also becoming more prominent. The peaks appear as flatter spectrum emission surrounded by regions where the spectral index decreases radially with increasing distance. Along the southern edge of the two lobes and the outer rim of the eastern one, there is evidence for spectral flattening of the limb. Also, fairly narrow bridges of emission with relatively flat spectra appear to link the central component and outer peaks.

The 3 km WSRT observations of DA240 show the two lobes and the radio core as completely distinct. Also, the distinction between the extended emission of the North-East lobe and its hot spot is clear. The hot spot is highly polarized, although the polarization structure is heavily distorted. In the remaining parts of the radio source there are a few small local peaks of polarization.

4C48.29. — Van Breugel and Jägers (1982) presented maps of 4C48.29 made with the WSRT at 4.9 GHz and 0.6 GHz. From the 4.9 GHz map it appears that the brightest components of the hot spots are well aligned with the radio core. Of the two components of the southern hot spot, the weakest is furthest away from the core. Bailey and Pooley (1968) noted that the parent galaxy of 4C48.29 is probably one of a pair of interacting galaxies.

The 3 km WSRT radio maps at 0.6 GHz show a clear difference in polarization structure between the northern and southern parts of 4C48.29. The northern part shows a lot of detailed structure whereas the southern part follows the large scale total intensity structure. The integrated degree of polarization of the southern part is more than three times greater than that of the northern part. There is hardly any depolarization (integrated) between 1.4 GHz and 0.6 GHz. The rotation of the polarization position angle between 1.4 GHz and 0.6 GHz is roughly constant over the radio source for the two outer edges of the southern part of the source.

The spectral index distribution in 4C48.29 exhibits in the North an increase in spectral index towards the West, in the South an increase towards the East and South.

IC708 AND IC711. — Vallée and Wilson (1976) showed the existence of two head-tail radio sources in the galaxy cluster Abell1314, IC708 and IC711 respectively, from observations of Abell1314 with the 1.5 km WSRT at 0.6 GHz and 5.0 GHz. At 5.0 GHz IC708 is resolved into a nuclear radio component and two radio jets extending to the West. The radio component ~ 1 arcmin South of the nucleus is probably not physically related to IC708. IC711, by way of contrast, shows a radio head with a single tail extending to the North-West. There is weak evidence for the existence of double radio structure close to the nucleus. At 0.6 GHz the tail has a length of ~ 15 arcmin.

Wilson and Vallée (1977) and Owen and Rudnick (1976) presented radio maps at 1.4 GHz and 2.7 GHz respectively. Vallée *et al.* (1979) showed « new » 5.0 GHz observations of IC708. They indicated that in the northern lobe of IC708 the magnetic field runs parallel to the western edge of the source while in the southern component it seems to curve in an arc, broadly following the contours of the total intensity brightness. The 3 km WSRT observations at 0.6 GHz show a few polarization peaks in IC708, the radio core and mainly the northern component. At 1.4 GHz the northern part is also stronger polarized than the southern part. The depolarization is large between 0.6 GHz and 1.4 GHz.

In IC711 only the head has a significant polarization peak, which also indicates large depolarization. As shown earlier by Wilson and Vallée (1977) the spectral index between 0.6 GHz and 1.4 GHz in IC711 shows a general increase along the tail from the head, with small

areas where the spectral index remains constant. Beyond ~ 7 arcmin from the head the 1.4 GHz radio map of IC711 shows a strong decrease in intensity which explains the disorderly run of spectral index as well as the large uncertainties.

4CT51.29. — Rudnick and Owen (1976, 1977) and Miley and Harris (1977) have observed 4CT51.29 at 2.7 GHz and 8.1 GHz and at 1.4 GHz respectively. Miley and Harris (1977) indicated that the unique curved structure in 4CT51.29 implies that the trajectory of the associated galaxy changed sharply on a scale of 100 kpc and/or that the galaxy is imbedded in a confining intergalactic wind which changes direction over this distance.

The 3 km WSRT observations at 0.6 GHz confirm the curve at the South-East of 4CT51.29 found by Miley and Harris (1977). The spectral index distribution between 0.6 GHz and 1.4 GHz shows that the spectrum at the northern tip of the western component is relatively flat compared with the southern part of the eastern component. This indicates that the former is relatively young, favouring the first explanation of the structure of 4CT51.29.

The polarization distribution at 0.6 GHz shows one strong peak south of the eastern component and a few weaker peaks along the edges of the maxima in the total intensity distribution. At 1.4 GHz the polarization peaks and the peaks in the total intensity distribution mostly coincide.

3C310. — 3C310 has previously been mapped at 5.0 GHz, 1.4 GHz and 0.6 GHz with the 1.5 km WSRT (Miley and Van der Laan, 1973 ; Van Breugel, 1980a ; Van Breugel and Jägers, 1982). The brightness distribution observed at 5.0 GHz is very complex and consists of several regions of enhanced emission (Van Breugel, 1980a). Van Breugel (1980a) proposed a model in which these knots are assumed to have been generated in the inner regions from which they moved outwards as ram pressure-confined plasmons. The relativistic particles in the low brightness regions must be replenished and/or reaccelerated and it is proposed that this is done in the knots.

The average spectrum between 1.4 GHz and 5.0 GHz in the northern lobe is flatter than that of the southern lobe.

The polarization intensity in 3C310 is highest at the boundaries of the hot spots around the hole and along the flux tube. The magnetic field is clearly circumferential.

The 3 km WSRT observations at 0.6 GHz show a polarization structure concentrated in the northwestern part of the radio source. The fractional polarization increases toward the edge. This polarization structure roughly coincides with that at 1.4 GHz. At the highest peaks in the polarized intensity the rotation of the polarization position angle between 0.6 GHz and 1.4 GHz is about zero as previously indicated by Van Breugel and Jägers (1982).

The steep spectrum region at the east is probably disturbed by instrumental effects.

ABELL2256. — The complex radio emission from the X-ray cluster Abell2256 has been mapped using the 1.5 km WSRT at 1.4 GHz (Bridle *et al.*, 1979) and at 0.6 GHz (Bridle and Fomalont, 1976). This showed that the cluster contains at least four and possibly eight head tail radio sources, an unusually steep spectrum radio source with a unique morphology, emission extending over a 1×0.3 Mpc area with a remarkably uniform spectral index between 0.6 GHz and 1.4 GHz, about 20 % linear polarization at 1.4 GHz and a relatively uniform magnetic field.

The 3 km WSRT observations at 0.6 GHz of Abell2256 do not give much more information than already was known. The most interesting result of this measurement is the total lack of linear polarization. Thus between 0.6 GHz and 1.4 GHz Abell2256 is completely depolarized, indicating the presence of substantial thermal material.

3C402. — Macdonald *et al.* (1968) and Miley and Van der Laan (1973) presented radio maps of 3C402 at 1.4 GHz. At this frequency 3C402 has two bright components and a weaker third one connected by diffuse bridges of emission. Both bright components coincide with a galaxy. The complex structure of 3C402 therefore seems to be the result of the superimposition of two radio galaxies. Miley and Van der Laan (1973) indicated that it is impossible to tell which of the two galaxies is identified with the individual radio features, apart from the two unresolved bright components. The spectral index distribution between 0.6 GHz (3 km WSRT) and 1.4 GHz (1.5 km WSRT) shows a combination of the spectral index distributions of a narrow edge-brightened double source (e.g. Paper II) and of a head-tail radio source (e.g. this Paper) with overlap occurring in the area around the southern bright peak. This peak may be the third peak of the triple source and the head of the head-tail source.

At 0.6 GHz, 3C402 is only locally polarized with most of the few peaks in the southern part of the source, close to the edges.

3C465. — 3C465 is the prototype wide angle tailed radio source. It has been frequently observed at various frequencies with different instruments (e.g. Riley and Branson, 1973 ; Van Breugel, 1980b ; Eilek *et al.*, 1984).

Van Breugel (1980b) showed that at 0.6 GHz at the end of both tails, which are visible at frequencies of 1.4 GHz and below, the radio structure bends sharply towards the line of symmetry (North-East to South-

West) and almost connects both tails. The projected magnetic field is directed along the tails and is indicative of a helical symmetry.

High resolution VLA maps (Eilek *et al.*, 1984) show an unresolved radio core and a jet directed North-West connected with the core. No counter jet is visible. On both sides, hot spots are present. They also present new X-ray maps of the surrounding cluster gas. The radio structure of 3C465 cannot be explained by any of the conventional models. They present new possibilities for the dynamics of this type of radio tailed source : the effect of a current in jets, and the interaction with cooling clouds in the cluster gas.

The 3 km WSRT observations of 3C465 at 0.6 GHz also show the sharp bends at the ends of the tails. The spectral index rises above 2.0 beyond these bends. From the core the spectral index continuously increases along the tails.

The 0.6 GHz radio maps of 3C465 show an appreciable amount of polarization with much detailed structure. In the eastwest tail the polarization peaks are situated along the central line whereas in the northsouth tail the peaks are closer to the eastern edge. There is only a small rotation of the polarization position angle along the source. The vectors shown in the figures are independent of one another.

The depolarization and the rotation of the polarization position angle between 0.6 GHz and 1.4 GHz can be grouped into a few separate regions in the radio source.

Acknowledgements.

I acknowledge the staff of the Westerbork Radio Telescope and the Reduction Group for their work on these observations. The Westerbork Radio Observatory is operated by the Netherlands Foundation for Radio Astronomy with the financial support of the Netherlands Organization for the Advancement of pure Research (ZWO). I acknowledge W. Brokaar and J. Ober for preparation of the figures.

References

Bailey, J. A., Pooley, G. G. : 1968, *Mon. Not. R. Astron. Soc.* **138,** 51.
Barthel, P. D., Schilizzi, R. T., Miley, G. K., Jägers, W. J., Strom, R. G. : 1984, Thesis, Rijks Universiteit Leiden, The Netherlands.
Bridle, A. H., Fomalont, E. B. : 1976, *Astron. Astrophys.* **52,** 107.
Bridle, A. H., Fomalont, E. B., Miley, G. K., Valentijn, E. A. : 1979, *Astron. Astrophys.* **80,** 201.
Butcher, H., Van Breugel, W. J. M., Miley, G. K. : 1980, *Astrophys. J.* **235,** 749.
Downes, A. : 1980, *Mon. Not. R. Astron. Soc.* **190,** 261.
Eilek, J. A., Burns, J. O., O'Dea, C. P., Owen, F. N. : 1984, *Astrophys. J.* **278,** 37.
Fomalont, J. A., Bridle, A. H., Miley, G. K. : 1982 in *Extragalactic Radio Sources, Proc. IAU Symp.* No. **97** (Reidel, Dordrecht, The Netherlands) p. 173.
Gisler, G. R., Miley, G. K. : 1979, *Astron. Astrophys.* **76,** 109.
Icke, V. : 1981, *Astrophys. J.* **246,** L65.
Jaffe, W. J., Perola, G. C. : 1973, *Astron. Astrophys.* **26,** 423.
Jägers, W. J., De Grijp, M. H. K. : 1983, *Astron. Astrophys.* **127,** 235.
Jägers, W. J. : 1987, *Astron. Astrophys. Suppl. Ser.* **67,** 395.
Jägers, W. J. : 1987a, *Astron. Astrophys. Suppl. Ser.* **71,** 75.
Leahy, J. P., Jägers, W. J., Pooley, G. G. : 1986, *Astron. Astrophys.* **156,** 234.
Macdonald, G. H., Kenderdine, S., Neville, A. C. : 1968, *Mon. Not. R. Astron. Soc.* **138,** 259.
Miley, G. K., Perola, G. C., Kruit, P. C., Van der Laan, H. : 1972, *Nature* **237,** 269.
Miley, G. K. : 1973, *Astron. Astrophys.* **26,** 413.
Miley, G. K., Van der Laan, H. : 1973, *Astron. Astrophys.* **38,** 359.
Miley, G. K., Wellington, K. J., Van der Laan, H. : 1975, *Astron. Astrophys.* **38,** 381.
Miley, G. K., Harris, D. E. : 1977, *Astron. Astrophys.* **61,** L23.
Miley, G. K. : 1980, *Ann. Rev. Astron. Astrophys.* **18,** 165.
Noordam, J. E., De Bruyn, A. F. : 1982, *Nature* **299,** 597.
Northover, K. J. E. : 1973, *Mon. Not. R. Astron. Soc.* **165,** 369.
Owen, F. N., Rudnick, L. : 1976, *Astrophys. J.* **205,** L3.
Owen, F. N., Burns, J. O., Rudnick, L. : 1978, *Astrophys. J. Lett.* **226,** L119.
Riley, J. M., Branson, N. J. B. A. : 1973, *Mon. Not. R. Astron. Soc.* **164,** 271.
Rudnick, L., Owen, F. N. : 1976, *Astrophys. J.* **203,** L107.
Rudnick, L., Owen, F. N. : 1979, *Astron. J.* **82,** 1.
Rudnick, L., Burns, J. O. : 1981, *Astrophys. J.* **246,** L69.
Strom, R. G., Willis, A. G. : 1980, *Astron. Astrophys.* **85,** 36.
Strom, R. G., Baker, J. R., Willis, A. G. : 1981, *Astron. Astrophys.* **100,** 220.

VALLÉE, J. P., WILSON, A. J. : 1976, *Nature* **259,** 451.
VALLÉE, J. P., WILSON, A. J., VAN DER LAAN, H. : 1979, *Astron. Astrophys.* **77,** 183.
VAN BREUGEL, W. J. M. : 1980a, *Astron. Astrophys.* **81,** 265.
VAN BREUGEL, W. J. M. : 1980b, *Astron. Astrophys.* **88,** 248.
VAN BREUGEL, W. : 1982, *Astron. Astrophys.* **110,** 225.
VAN BREUGEL, W., JÄGERS, W. : 1982, *Astron. Astrophys. Suppl. Ser.* **49,** 529.
WILSON, A. J., VALLÉE, J. P. : 1977, *Astron. Astrophys.* **58,** 79.

TABLE I. — *Observational parameters.*

Source	Alternative Name	Field Centre RA(1950) H M S	Field Centre DEC(1950) D M S	Field Centre l D	Field Centre b D	Observing Date YR Day	Receiver	Interferometer Configuration M			Halfpower Beam(arcs) RA x DEC	RMS Noise mJy/bm	Confusion Level mJy/bm
(1)	(2)	(3)	(4)	(5)	(6)	(7)	(8)	(9)	(10)	(11)	(12)	(13)	(14)
0219+427	3C66B	02 19 30	42 26 00	140.3	-17.1	80 316	old	36	36	2736	29 x 43	0.7	10.0
		02 19 30	42 26 00	140.3	-17.1	80 323	old						
0314+416	NGC1265	03 15 00	41 50 00	150.1	-13.0	80 328	old	72	72	2736[a]	29 x 44	0.5	10.0
		03 15 00	41 30 00	150.1	-13.3	80 012	new	72	72	2736	29 x 44		
0445+449	3C129	04 44 45	44 55 00	160.3	0.0	80 322	old	72	72	2736	29 x 41	1.1	5.0
0744+559	DA240	07 44 40	55 52 00	162.0	30.1	82 083	new	72	72	2736	29 x 35	0.4	2.0
1003+351	3C236	10 03 15	35 07 00	190.1	54.0	82 024/032	new	72	72	2736	29 x 50	0.6	5.0
1017+497	4C48.29	10 18 00	48 45 00	166.3	54.0	82 075	new	72	72	2736	29 x 39	0.4	4.0
1131+492	IC708/711	11 31 40	49 18 00	152.0	63.5	82 022	new	72	72	2736	29 x 38	0.4	2.0
1200+519	4CT51.29.1	12 00 30	51 56 00	140.1	63.8	82 077	new	72	72	2736	29 x 37	0.4	2.5
1502+262	3C310	15 02 48	26 12 00	38.5	60.2	81 169	old	36	36	2736	29 x 66	0.9	10.0
		15 02 48	26 12 00	38.5	60.2	82 055	new						
1806+787	Abell2256	17 06 00	78 45 00	111.1	31.8	82 013/032	new	72	72	2736	29 x 30	0.6	2.5
1940+504	3C402	19 40 18	50 29 00	83.4	13.3	81 171	old	72	72	2736	29 x 38	1.1	4.0
2335+267	3C465	23 36 00	26 43 59	193.5	-33.1	82 019	new	72	72	2736	29 x 64	0.7	15.0

a - Redundancy mode

TABLE II. — *Relevant parameters of the additional 1.4* GHz *observations.*

Source	Alternative Name	Frequency and Bandwidth MHZ	MHZ	Year of Observation	RMS Noise mJy/beam	Confusion Level I-map mJy/beam	Notes
(1)	(2)	(3)	(4)	(5)	(6)	(7)	(8)
0219+427	3C66B	1415	4	1975	0.2	5.0	a
0314+416	NGC1265	1412	10	1982	0.2	2.5	b
0445+449	3C129	1415	4	1971	0.5	2.5	c
0744+559	DA240						d
1003+351	3C236						d
1017+497	4C48.29	1415	4	1977	0.3	2.0	a
1131+492	IC708/711	1415	4	1974/1975	0.2	1.0	e
1200+519	4CT51.29.1	1415	4	1975	0.4	2.0	f
1502+262	3C310	1415	4	1971	1.0	5.0	g
1706+787	Abell 2256	1415	4	1975	0.2	0.75	h
1940+504	3C402	1412	10	1977/1978	0.3	3.0	g
2335+267	3C465	1415	4	1972	1.0	5.0	g

Notes to Table

(a) Van Breugel, W., Jägers, W. : 1982, *Astron. Astrophys. Suppl. Ser.* **49,** 529.
(b) unpublished 3 km WSRT observation (see text).
(c) Miley, G. K. : 1973, *Astron. Astrophys.* **26,** 413.
(d) no useful 1.4 observations.
(e) Wilson, A. S., Vallee, J. P. : 1977, *Astron. Astrophys.* **58,** 79.
(f) Miley, G. K., Harris, D. E. : 1977, *Astron. Astrophys.* **61,** c23.
(g) Miley, G. K., Van der Laan, H. : 1973, *Astron. Astrophys.* **28,** 359.
(h) Bridle, A. M., Fomalont, E. B., Miley, G. K., Valentijn, E. A. : 1979, *Astron. Astrophys.* **80,** 201.

TABLE III. — *Integrated values.*

Source	Alternative Name	0.6 GHz Total Flux Density Jy	0.6 GHz Percentage Polarization %	0.6 GHz Polarization Position Angle Degrees	1.4 GHz Total Flux Density Jy	1.4 GHz Percentage Polarization %	1.4 GHz Polarization Position Angle Degrees
(1)	(2)	(3)	(4)	(5)	(6)	(7)	(8)
0219+427	3C66B	13.16 ± 0.35	0.4 ± 0.2	127 ± 13	7.46 ± 0.17	0.9 ± 0.1	54 ± 3
0314+416	NGC1265	12.10 ± 0.32	0.3 ± 0.1	65 ± 10	6.55 ± 0.08	1.5 ± 0.1	173 ± 1
0445 +449	3C129	14.41 ± 0.22	< 0.6	(80 ± 31)	7.03 ± 0.11	3.7 ± 0.3	45 ± 2
0744+559	DA240	6.38 ± 0.20	6.4 ± 1.3	167 ± 4			
1003+351	3C236	9.17 ± 0.23	1.2 ± 0.3	92 ± 6			
1017+497	4C48.29	3.10 ± 0.10	4.4 ± 0.3	30 ± 2	1.69 ± 0.05	5.1 ± 0.5	119 ± 3
1131+492	IC708	1.43 ± 0.03	< 0.6	(167 ± 152)	0.87 ± 0.01	1.1 ± 0.3	17 ± 11
	IC711	0.81 ± 0.04	< 1.5	(99 ± 51)	0.43 ± 0.02	2.6 ± 1.1	38 ± 18
1200+519	4CT51.27	1.08 ± 0.05	< 0.8	(100 ± 67)	0.62 ± 0.04	1.5 ± 0.2	55 ± 3
1502+262	3C310	19.71 ± 0.28	0.3 ± 0.1	72 ± 7	7.38 ± 0.14	1.4 ± 0.2	155 ± 4
1706+787	Abell 2256	1.19 ± 0.11	< 3.5	(135 ± 39)	0.42 ± 0.03	1.8 ± 0.8	22 ± 12
1940+504	3C402	5.53 ± 0.11	< 0.7	(123 ± 112)	2.93 ± 0.08	1.1 ± 0.2	154 ± 6
2335+267	3C465	15.86 ± 0.60	0.5 ± 0.1	43 ± 5	7.75 ± 0.20	0.5 ± 0.3	127 ± 15

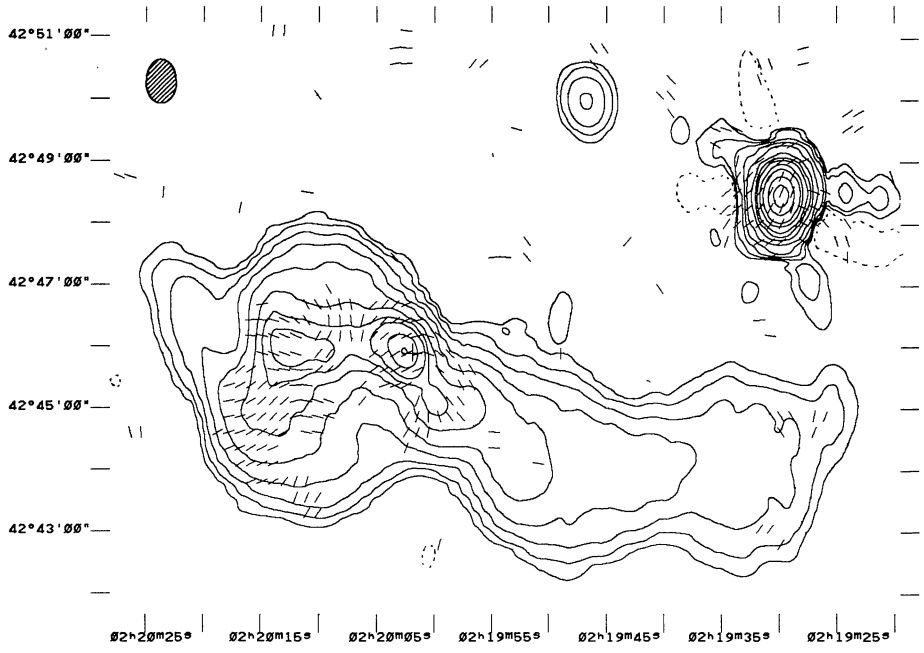

FIGURE 1a. — The total intensity distribution of 3C66B at 0.6 GHz. The contour levels are – 10, 10, 20, 40, 80, 160, 320, 480, 640, 960, 1280 and 1920 mJy/beam.

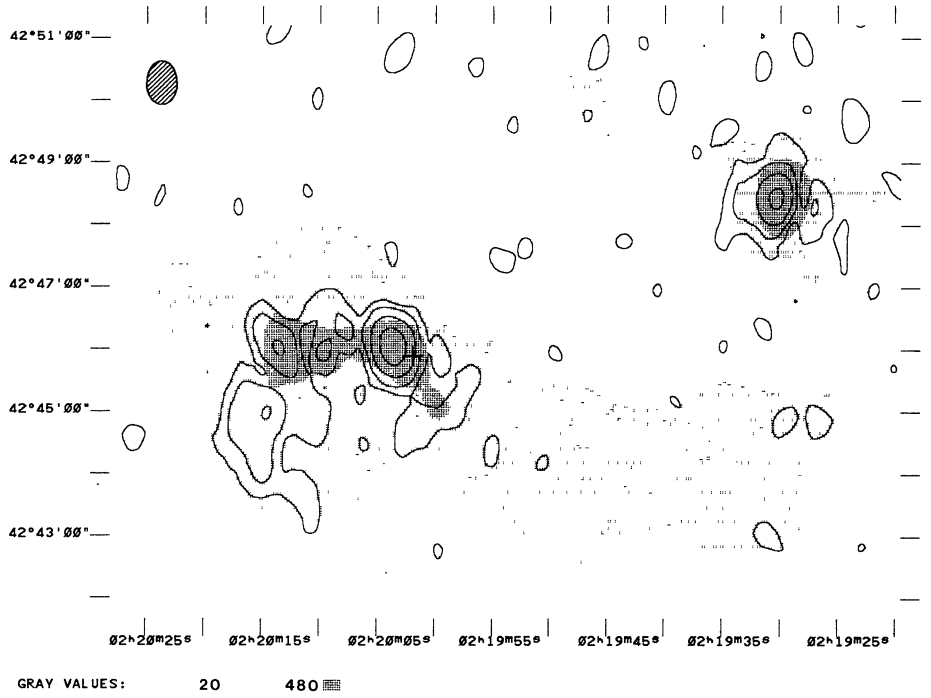

FIGURE 1b. — The linearly polarized intensity distribution of 3C66B at 0.6 GHz. The contour levels are 2.5, 5, 10 and 20 mJy/beam.

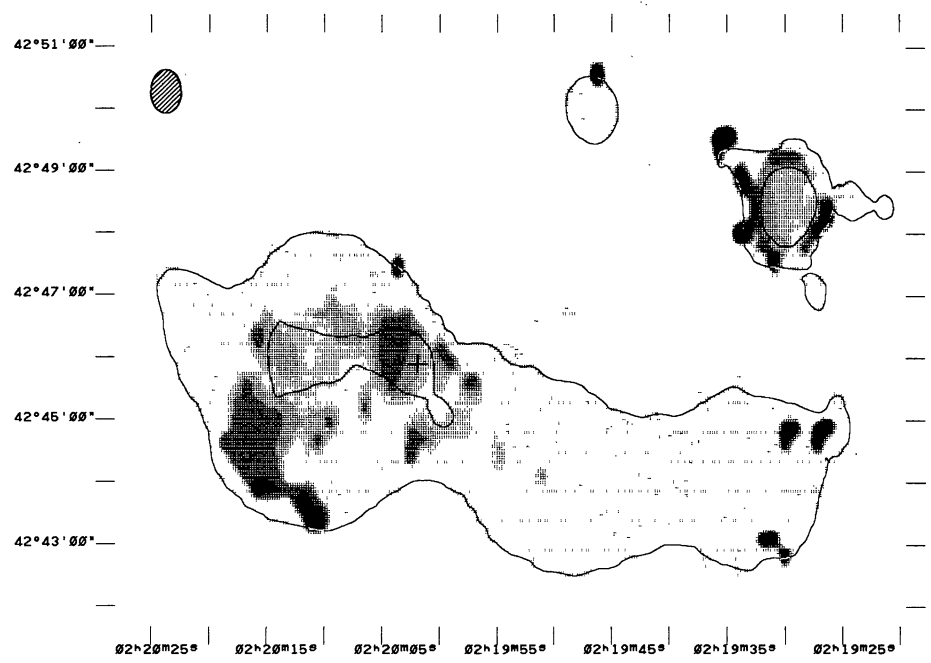

FIGURE 1c. — The distribution of the percentage polarization of 3C66B at 0.6 GHz. The two levels in the total intensity contour map are 20 and 480 mJy/beam.

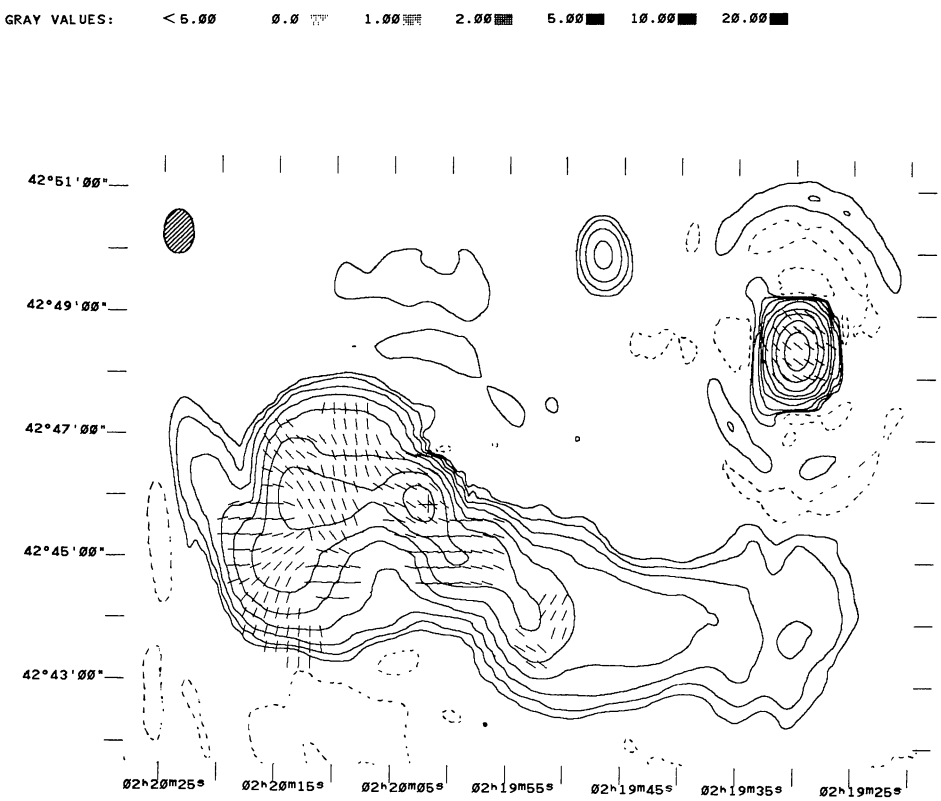

FIGURE 1d. — The total intensity distribution of 3C66B at 1.4 GHz. The contour levels are – 5, 5, 10, 20, 40, 80, 160, 320, 640 and 1280 mJy/beam.

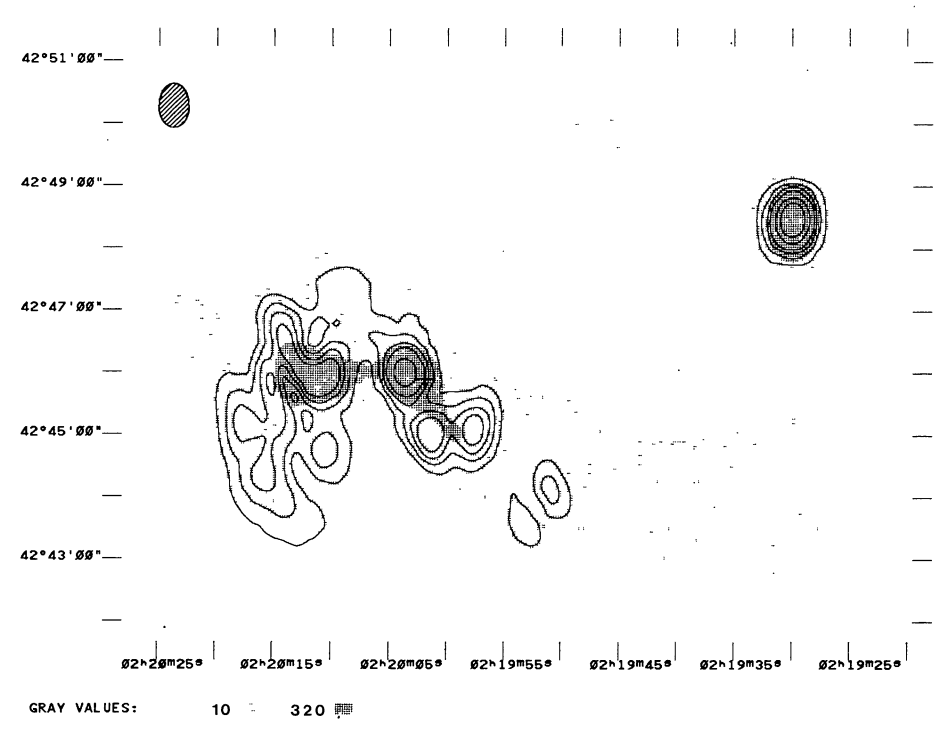

FIGURE 1e. — The linearly polarized intensity distribution of 3C66B at 1.4 GHz. The contour levels are 5, 10, 15, 20, 30 and 40 mJy/beam.

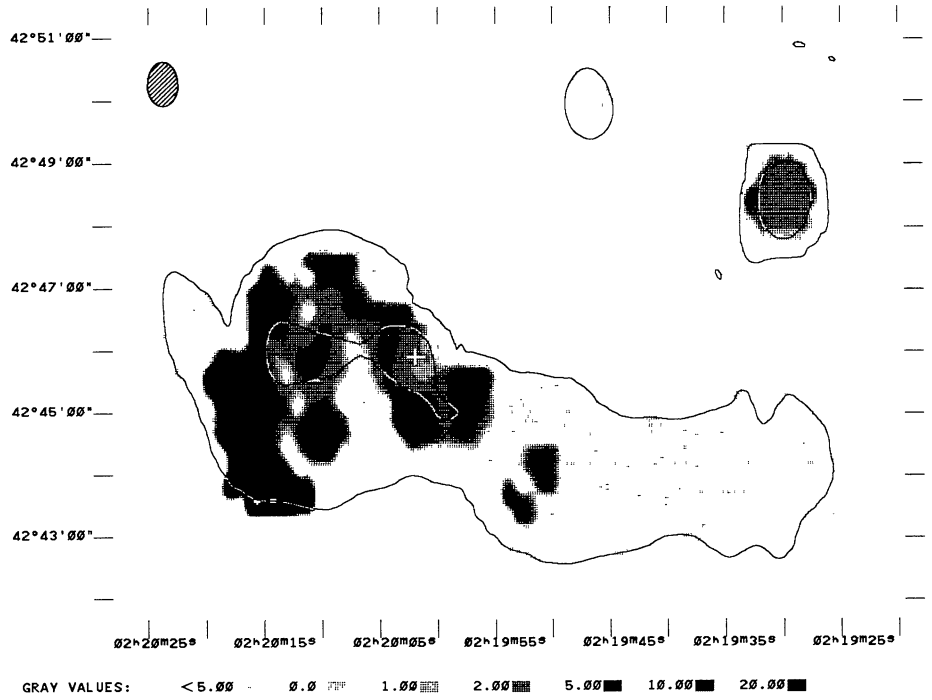

FIGURE 1f. — The distribution of the percentage polarization of 3C66B at 1.4 GHz. The two levels in the total intensity contour map are 10 and 320 mJy/beam.

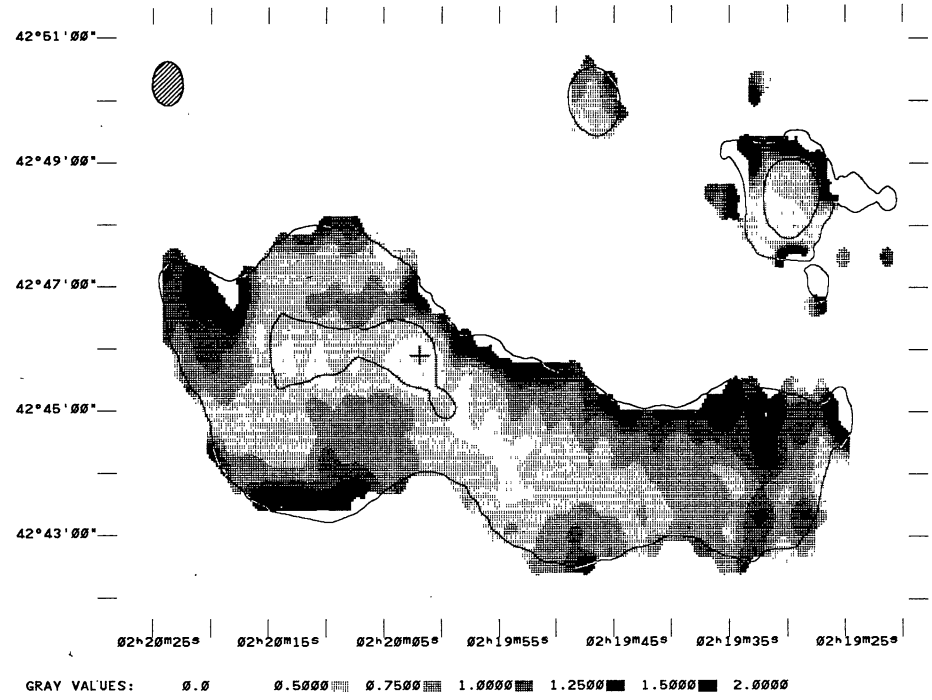

FIGURE 1g. — The distribution of the spectral index of 3C66B between 0.6 GHz and 1.4 GHz. The two levels in the total intensity contour map at 0.6 GHz are 20 and 480 mJy/beam.

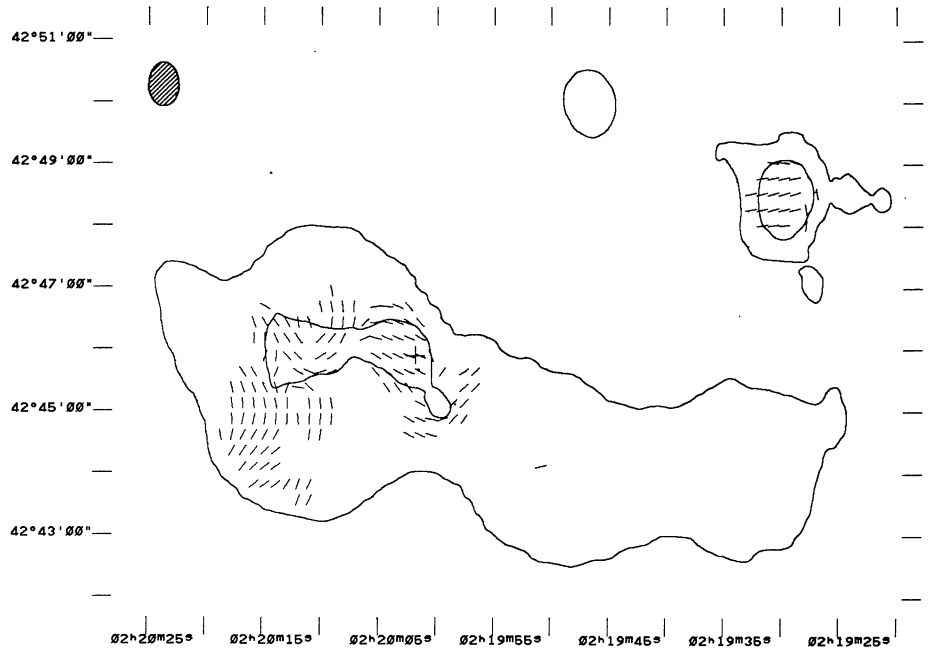

FIGURE 1h. — The distribution of the depolarization of 3C66B between 0.6 GHz and 1.4 GHz. The two levels in the total intensity contour map at 0.6 GHz are 20 and 480 mJy/beam.

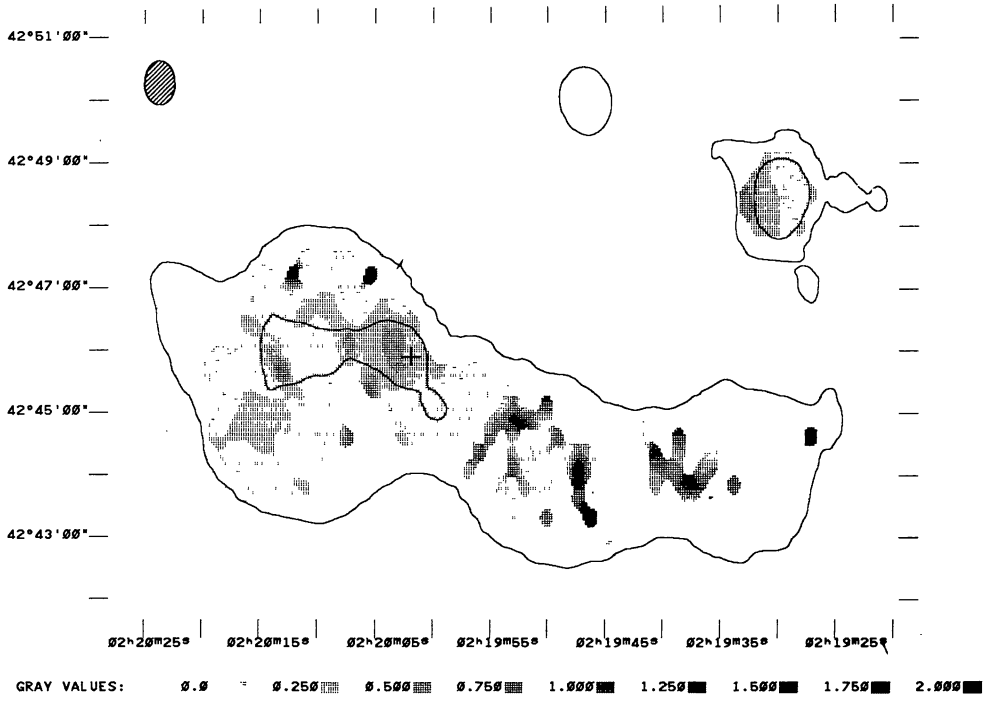

FIGURE 1i. — The distribution of the rotation of the polarization position angle of 3C66B between 0.6 GHz and 1.4 GHz measured from the North towards the East. The two levels in the total intensity contour map at 0.6 GHz and at 1.4 GHz are 20 and 480 mJy/beam.

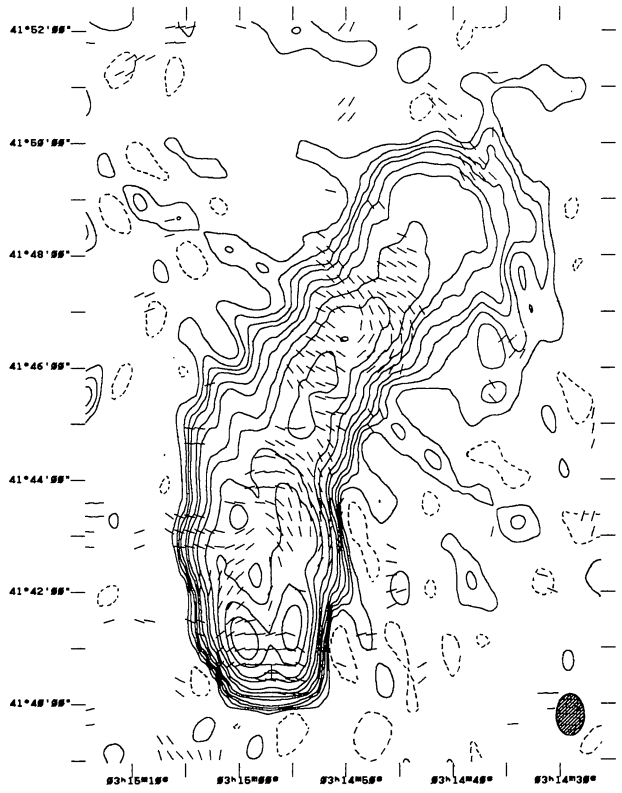

FIGURE 2a. — The total intensity distribution of NGC 1265 at 0.6 GHz. The contour levels are – 10, 10, 20, 30, 40, 60, 80, 120, 160, 240, 320, 480 and 640 mJy/beam.

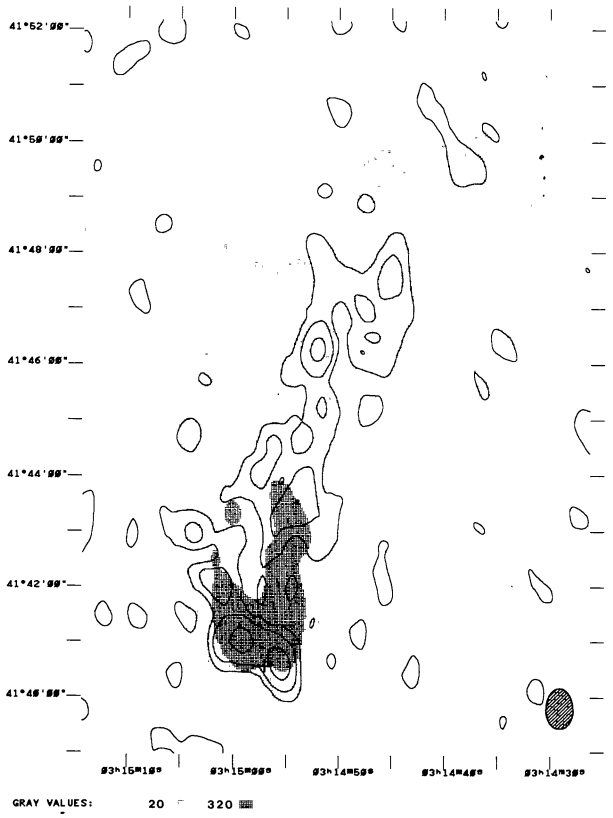

FIGURE 2b. — The linearly polarized intensity distribution of NGC 1265 at 0.6 GHz. The contour levels are 5, 10, 20 and 40 mJy/beam.

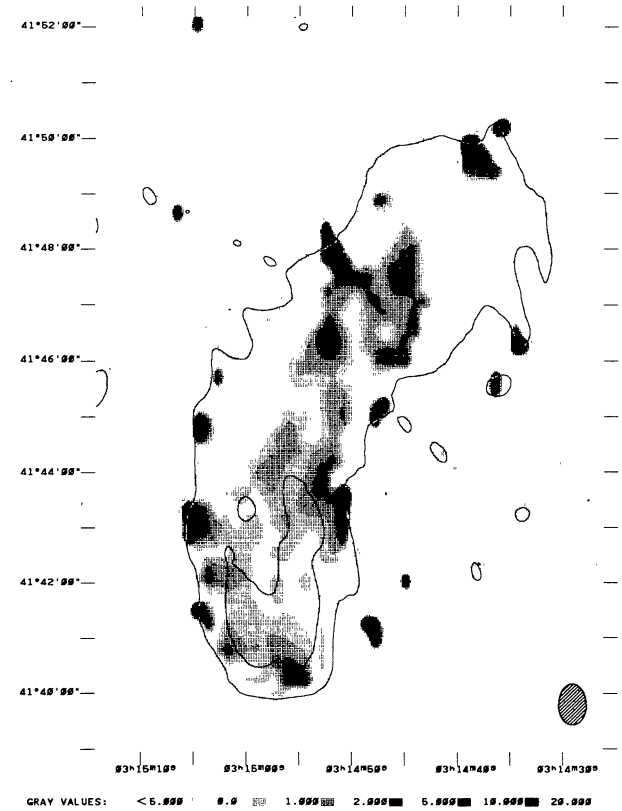

FIGURE 2c. — The distribution of the percentage polarization of NGC 1265 at 0.6 GHz. The two levels in the total intensity contour map are 20 and 320 mJy/beam.

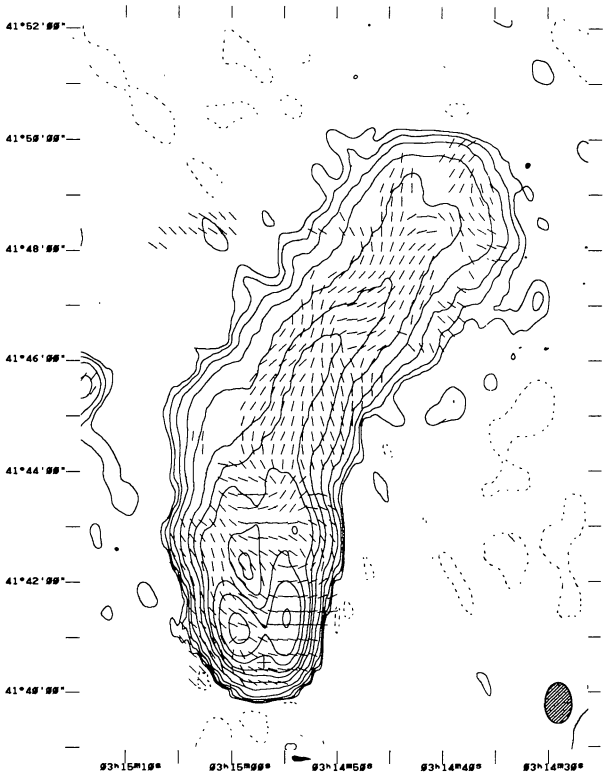

FIGURE 2d. — The total intensity distribution of NGC 1265 at 1.4 GHz. The contour levels are – 5, 5, 10, 20, 40, 80, 120, 160, 240, 320, 480 and 640 mJy/beam.

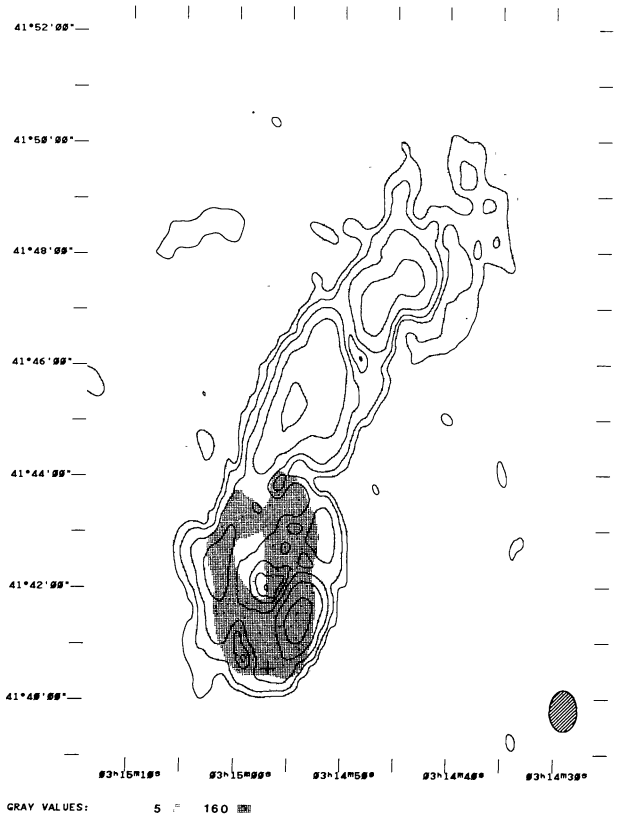

FIGURE 2e. — The linearly polarized intensity distribution of NGC 1265 at 1.4 GHz. The contour levels are 3/4.75, 1.5, 3, 6, 12, 24 and 36 mJy/beam.

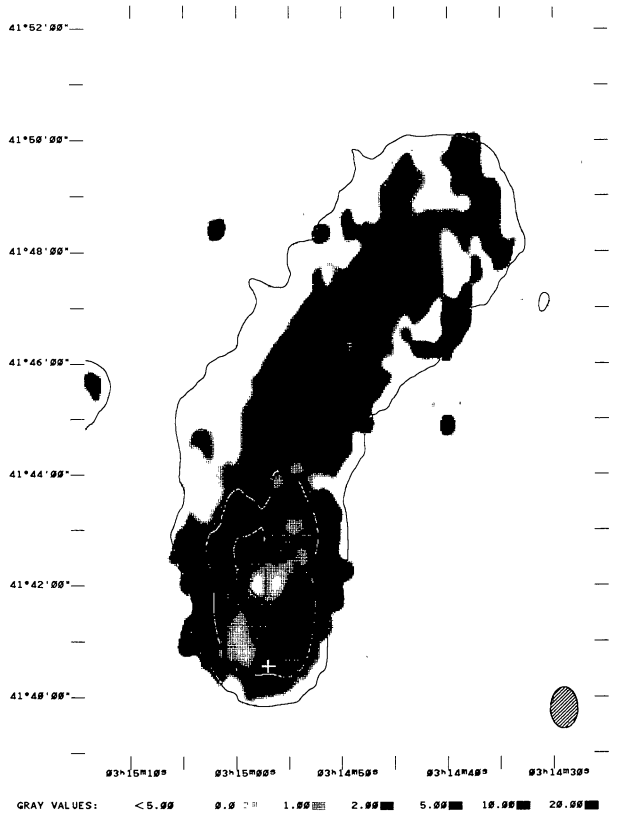

FIGURE 2f. — The distribution of percentage polarization of NGC 1265 at 1.4 GHz. The two levels in the total intensity contour map are 10 and 160 mJy/beam.

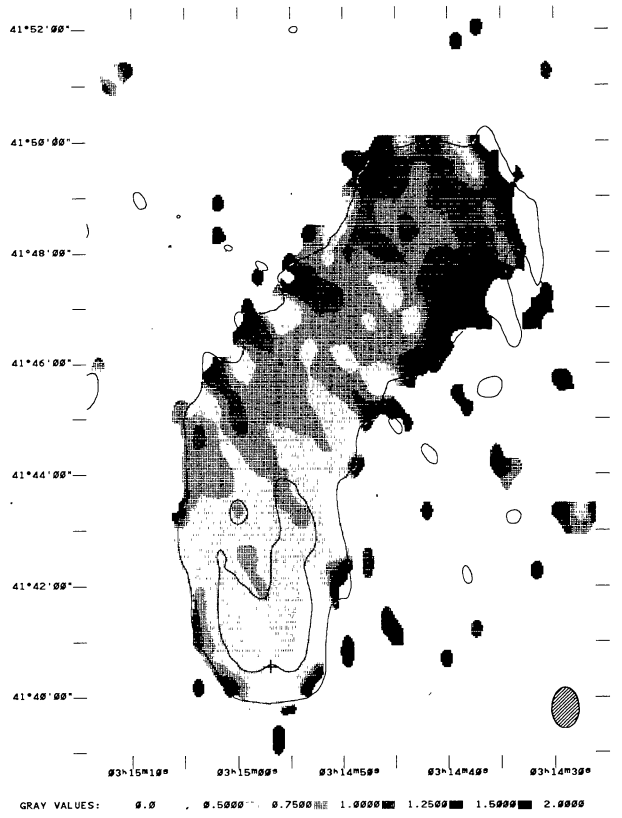

FIGURE 2g. — The distribution of the spectral index of NGC 1265 between 0.6 GHz and 1.4 GHz. The two levels in the total intensity contour map at 0.6 GHz are 20 and 320 mJy/beam.

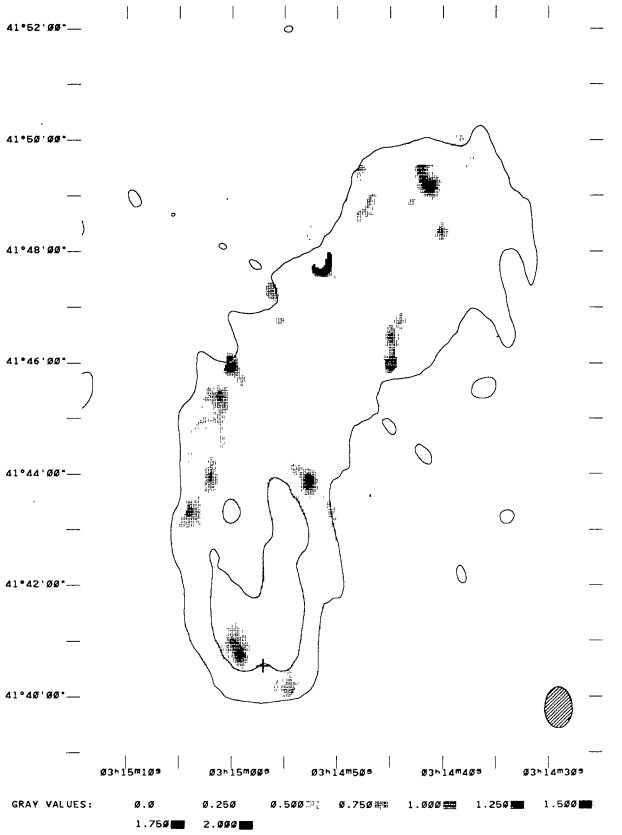

FIGURE 2h. — The distribution of the depolarization of NGC 1265 between 0.6 GHz and 1.4 GHz. The two levels in the total intensity contour map at 0.6 GHz are 20 and 320 mJy/beam.

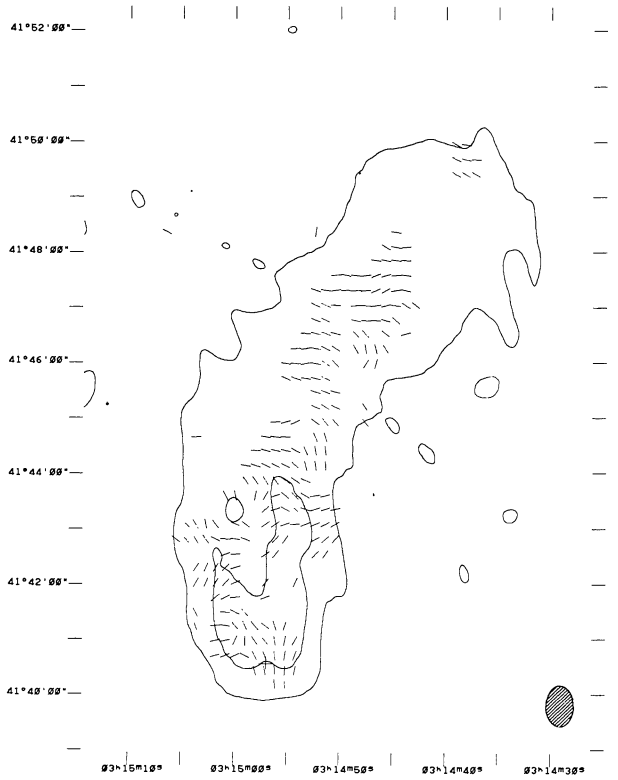

FIGURE 2i. — The distribution of the rotation of the polarization position angle of NGC 1265 between 0.6 GHz and 1.4 GHz measured from the North towards the East. The two levels in the total intensity contour map at 0.6 GHz are 20 and 320 mJy/beam.

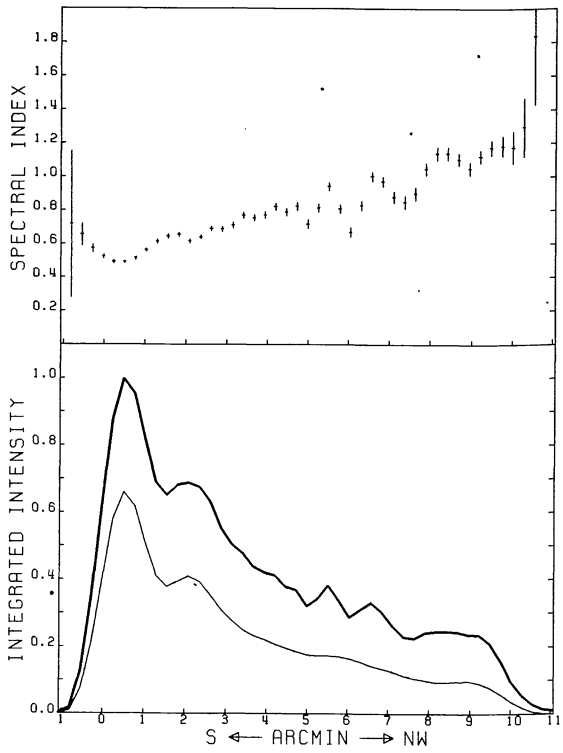

FIGURE 2j. — The spectral index variations along the major axis of NGC 1265 between 0.6 GHz and 1.4 GHz. The lower panel shows the integrated total intensity along the radio source at 0.6 GHz (thick line) and 1.4 GHz (thin line). The upper panel shows the variations of the spectral index along the radio source.

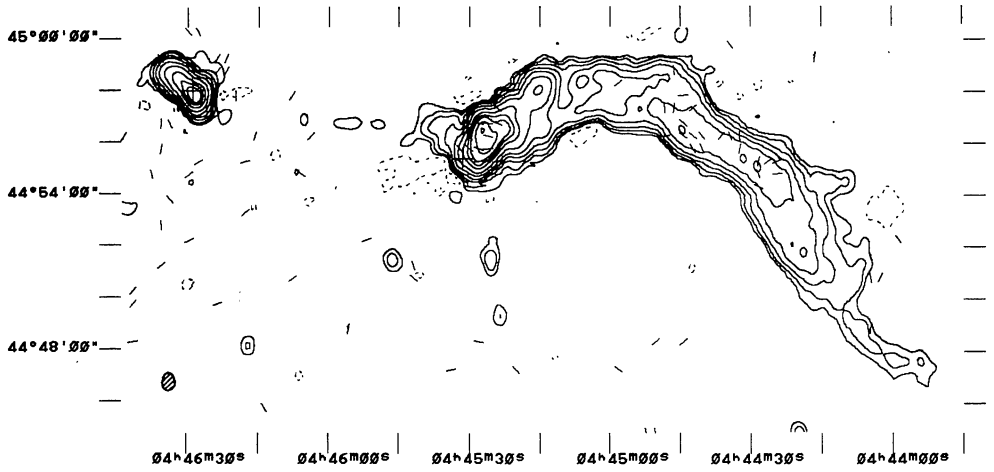

FIGURE 3a. — The total intensity distribution of 3C129 at 0.6 GHz. The contour levels are – 5, 5, 10, 20, 40, 80, 160, 320, 480, 640, 960 and 1280 mJy/beam.

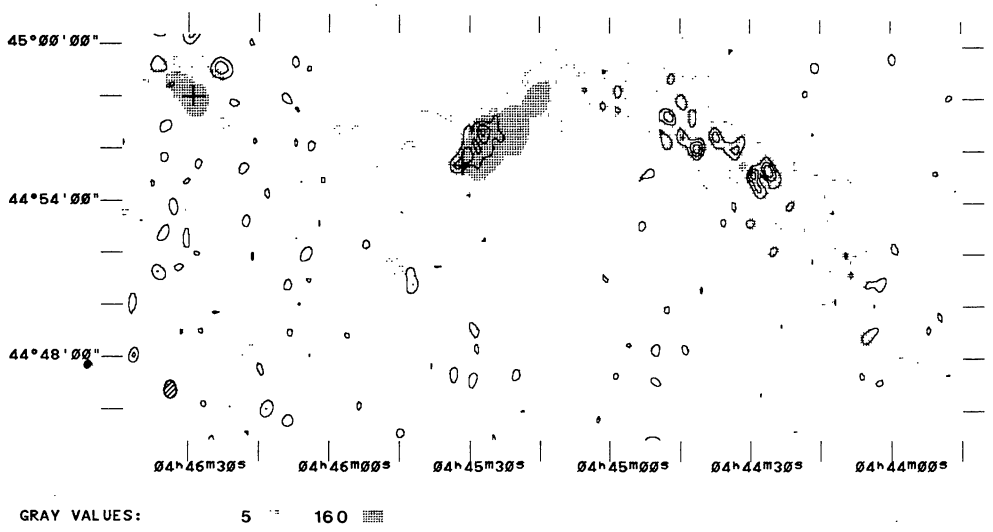

FIGURE 3b. — The linearly polarized intensity distribution of 3C129 at 0.6 GHz. The contour levels are 3, 4.5 and 6 mJy/beam.

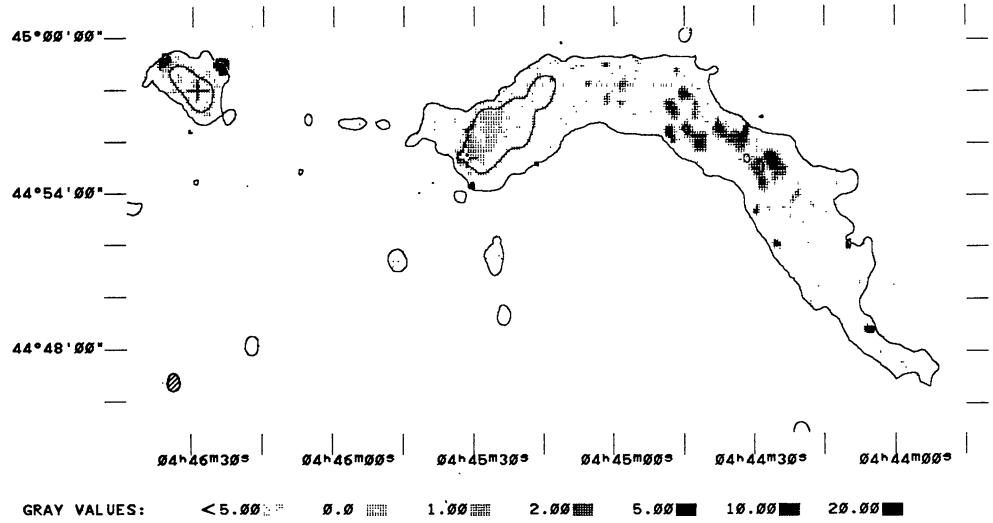

FIGURE 3c. — The distribution of the percentage polarization of 3C129 at 0.6 GHz. The two levels in the total intensity contour map are 5 and 160 mJy/beam.

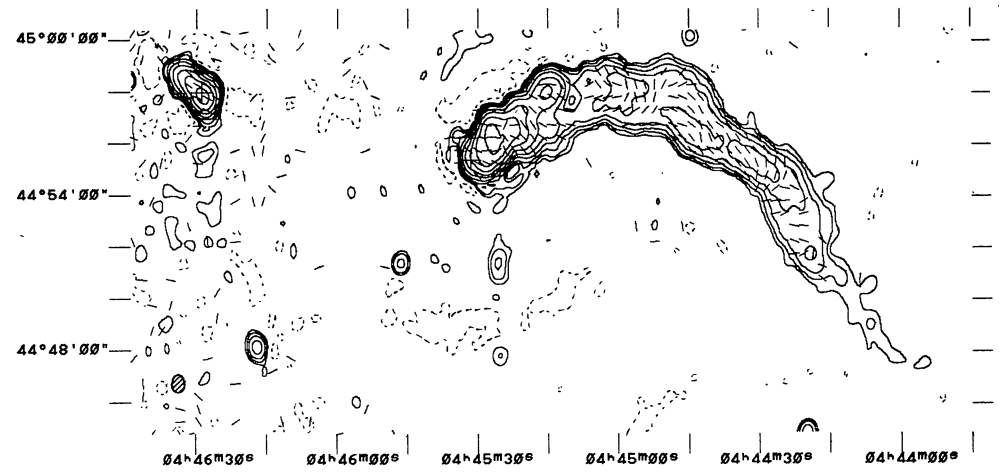

FIGURE 3d. — The total intensity distribution of 3C129 at 1.4 GHz. The contour levels are – 2.5, 2.5, 5, 10, 20, 40, 80, 160, 320 and 640 mJy/beam.

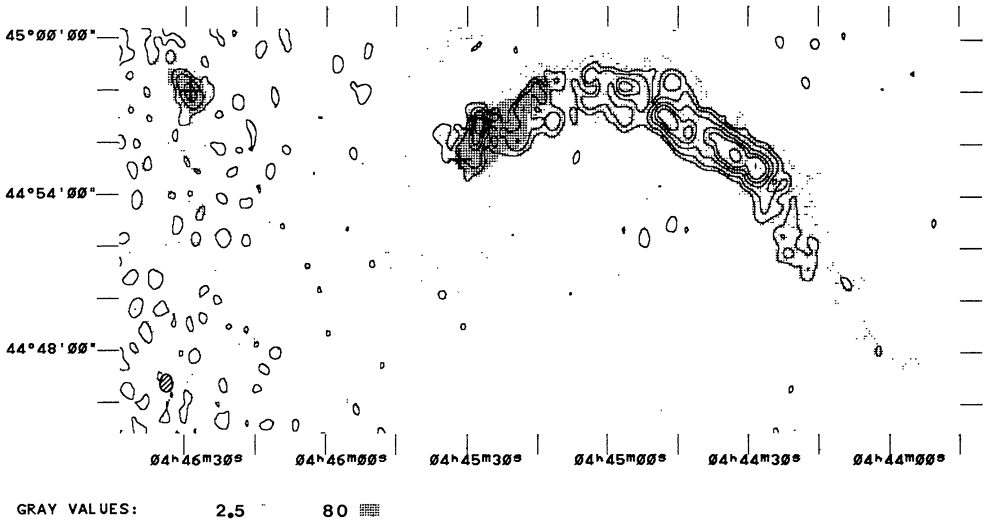

FIGURE 3e. — The linearly polarized intensity distribution of and 3C129 at 1.4 GHz. The contour levels are 2.5, 5, 10, 15, 20 and 30 mJy/beam.

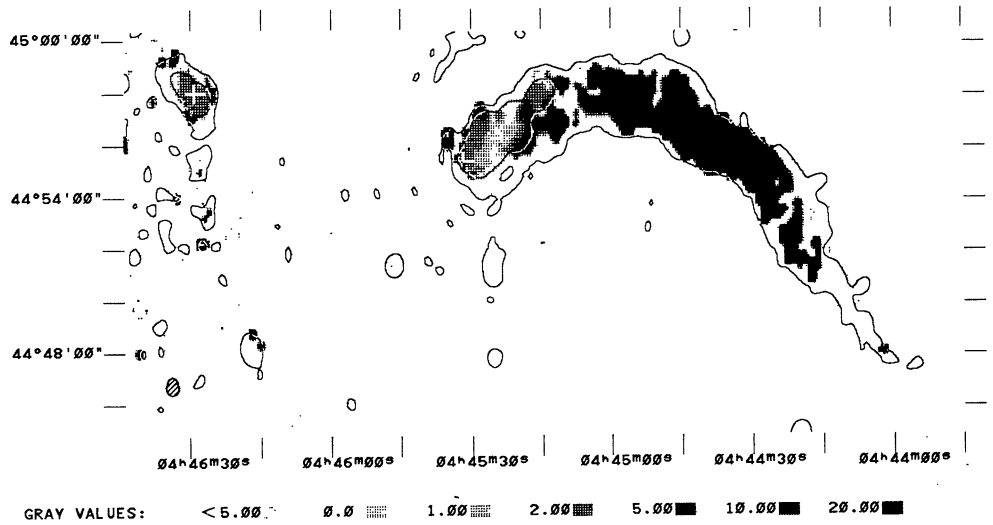

FIGURE 3f. — The distribution of the percentage polarization of 3C129 at 1.4 GHz. The two levels in the total intensity contour map are 2.5 and 80 mJy/beam.

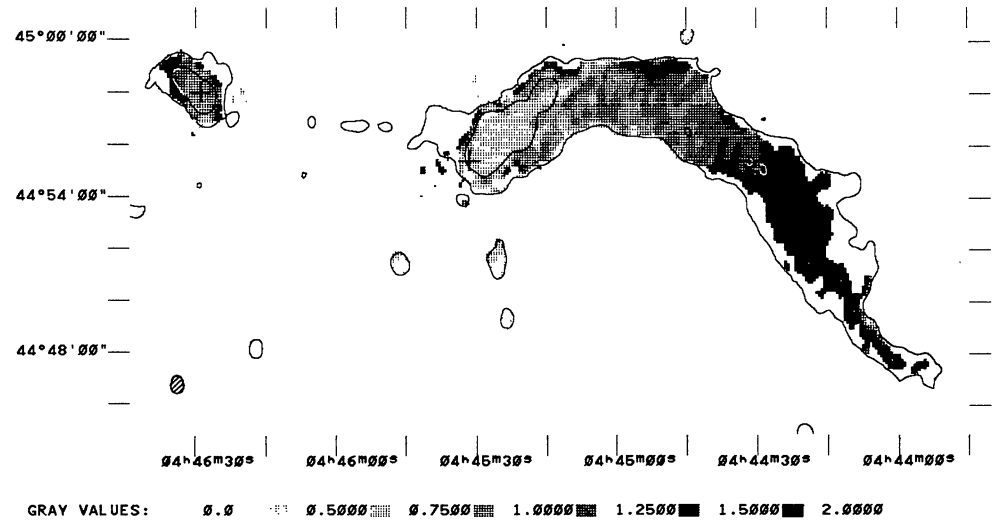

FIGURE 3g. — The distribution of the spectral index of 3C129 between 0.6 GHz and 1.4 GHz. The two levels in the total intensity contour map at 0.6 GHz are 5 and 160 mJy/beam.

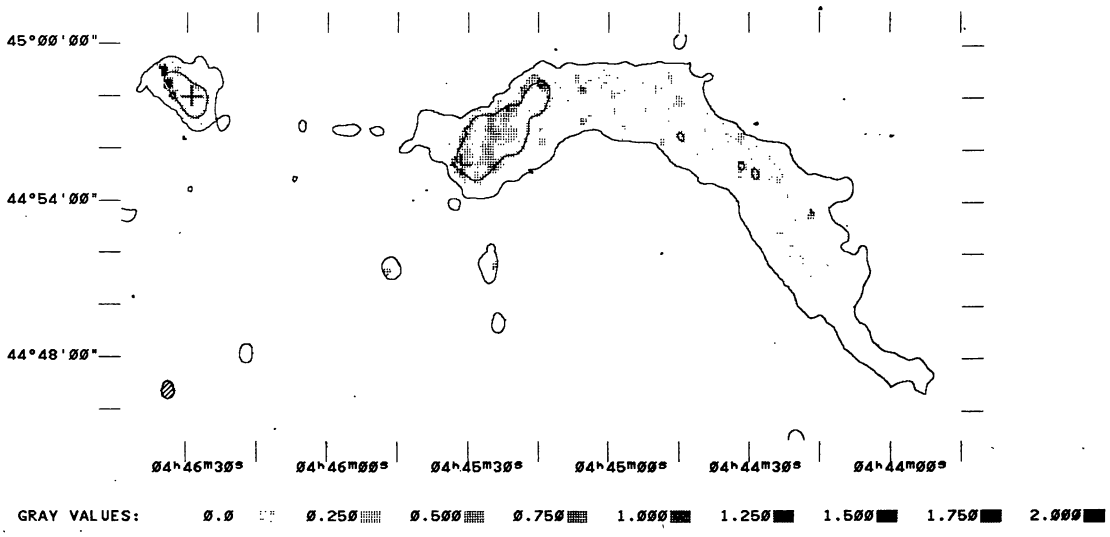

FIGURE 3h. — The distribution of the depolarization of 3C129 between 0.6 GHz and 1.4 GHz. The two levels in the total intensity contour map at 0.6 GHz are 5 and 160 mJy/beam.

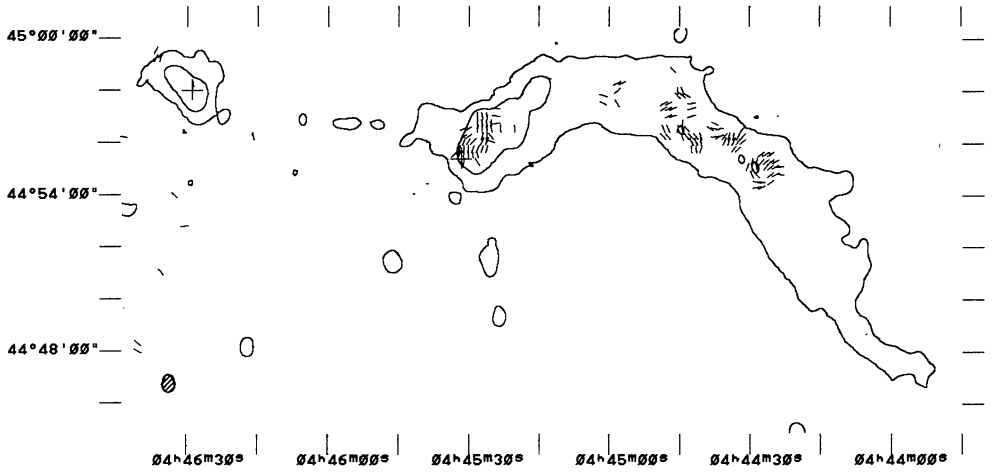

FIGURE 3i. — The distribution of the rotation of the polarization position angle of 3C129 between 0.6 GHz and 1.4 GHz measured from the North towards the East. The two levels in the total intensity contour map at 0.6 GHz are 5 and 160 mJy/beam.

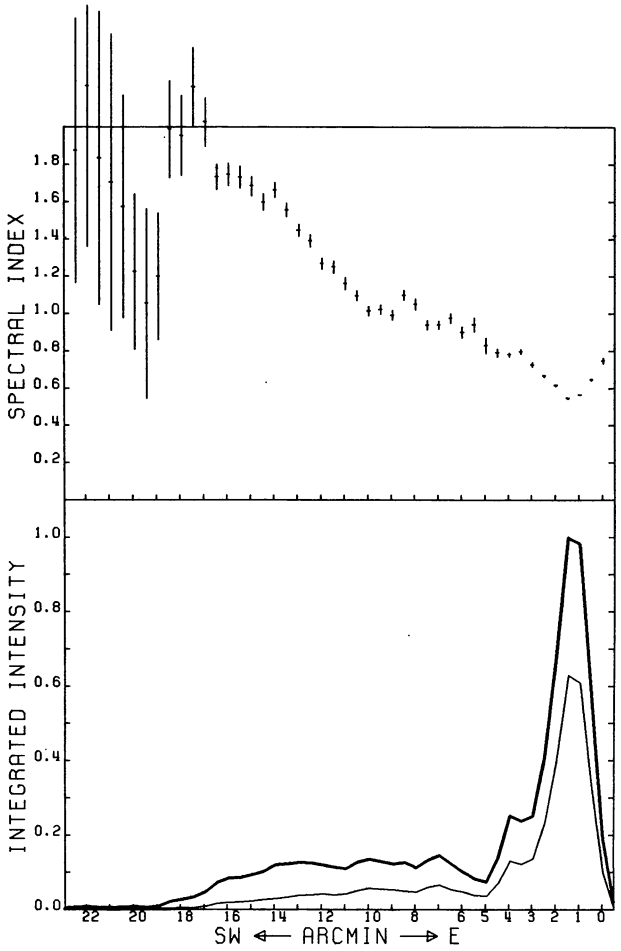

FIGURE 3j. — The spectral index variations along the major axis of 3C129 between 0.6 GHz and 1.4 GHz. The lower panel shows the (integrated) total intensity along the radio source at 0.6 GHz (thick line) and at 1.4 GHz (thin line). The upper panel shows the variations of the spectral index along the radio source.

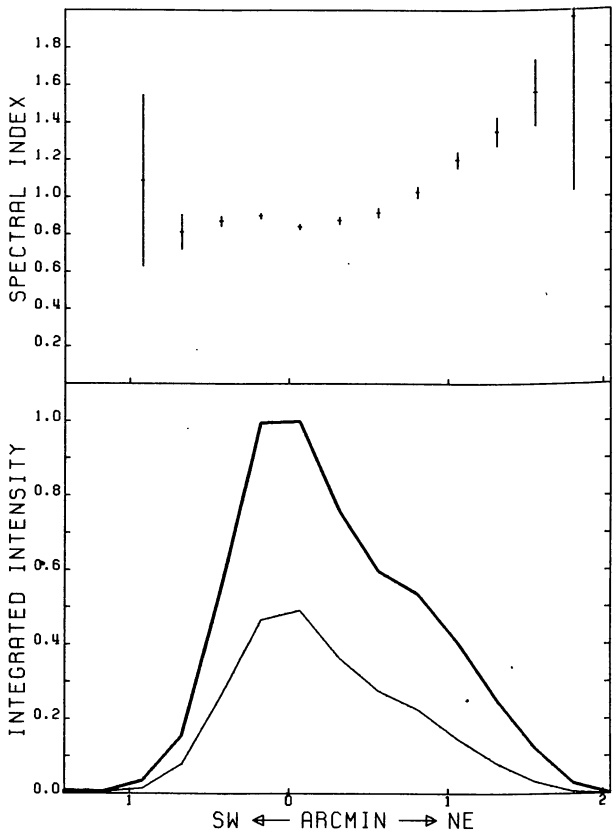

FIGURE 3k. — The spectral index variations along the major axis of 3C129.1 between 0.6 GHz and 1.4 GHz. The lower panel shows the (integrated) total intensity along the radio source at 0.6 GHz (thick line) and at 1.4 GHz (thin line). The upper panel shows the variations of the spectral index along the radio source.

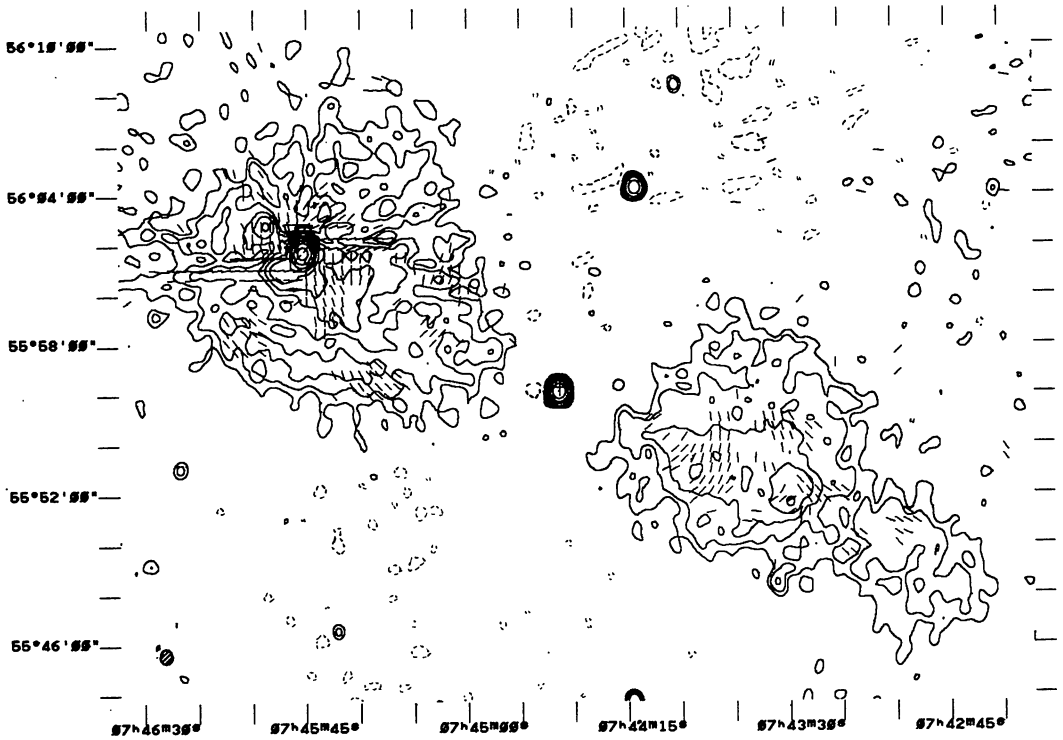

FIGURE 4a. — The total intensity distribution of DA240 at 0.6 GHz. The contour levels are – 3, 2, 4, 8, 16, 32, 64, 128, 256, 512 and 1024 mJy/beam.

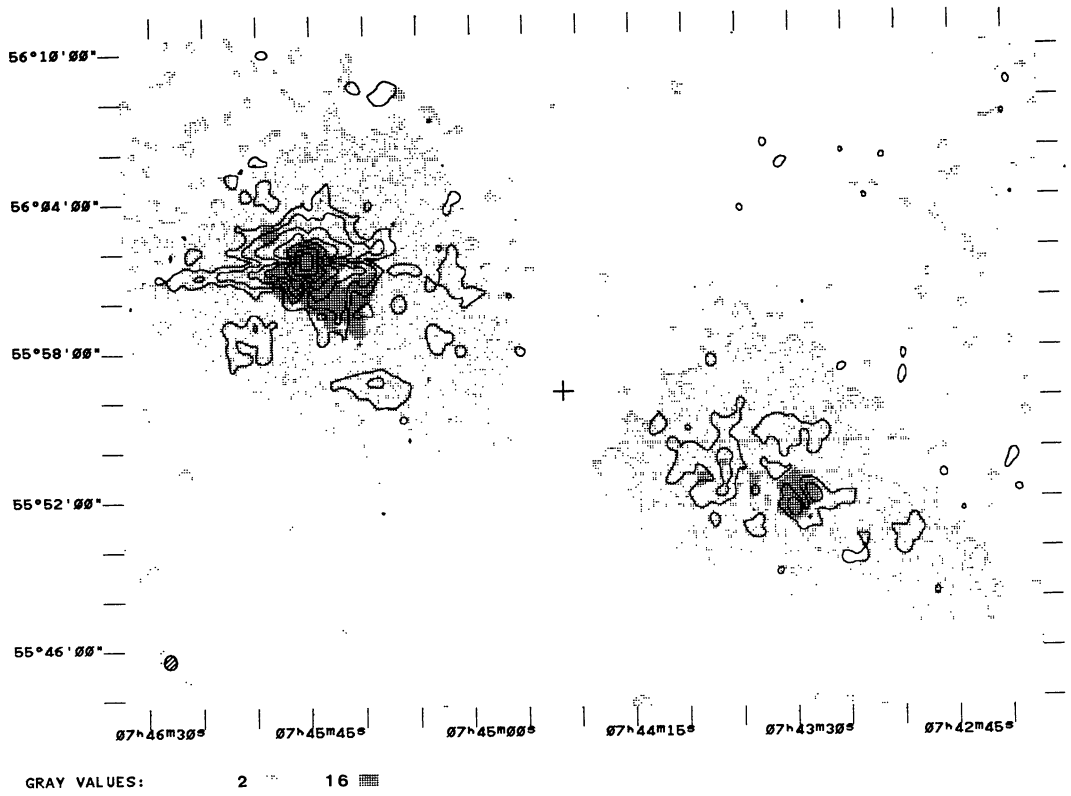

FIGURE 4b. — The linearly polarized intensity distribution of DA240 at 0.6 GHz. The contour levels are 2, 4, 8, 16, 32, 64 and 128 mJy/beam.

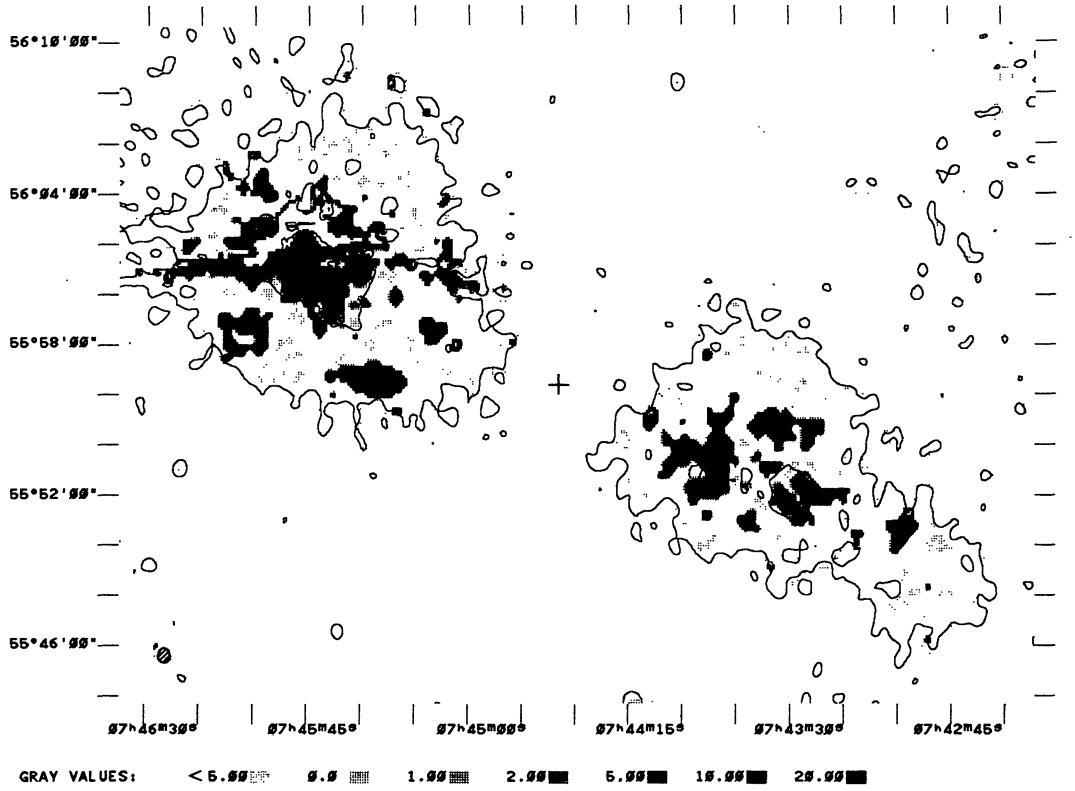

FIGURE 4c. — The distribution of DA240 at 0.6 GHz. The two levels in the total intensity contour map are 2 and 16 mJy/beam.

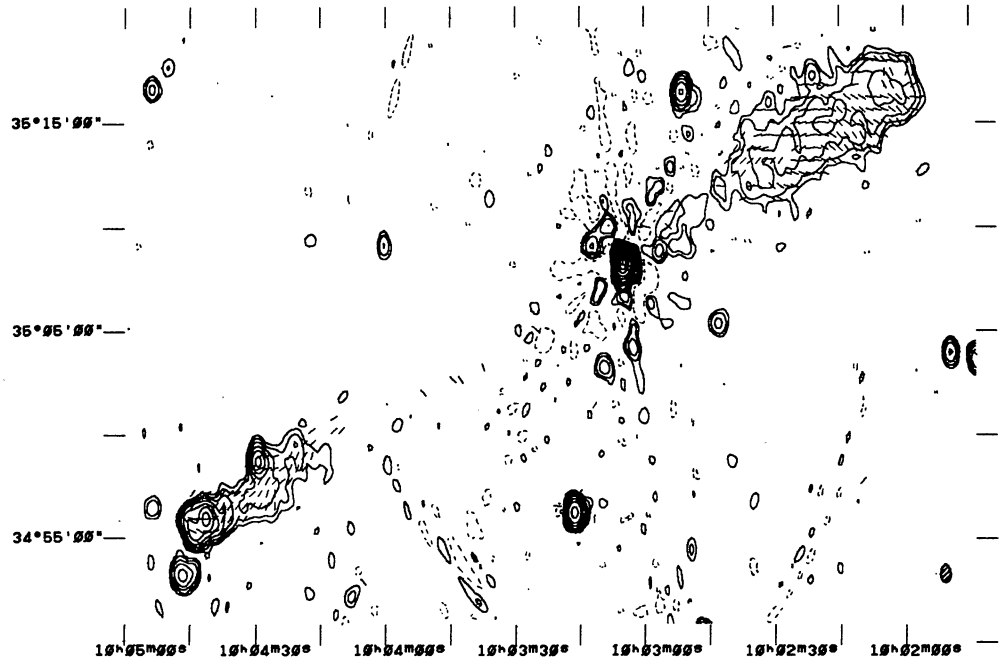

FIGURE 5a. — The total intensity distribution of 3C236 at 0.6 GHz. The contour levels are – 3, 2, 4, 8, 16, 32, 64, 128, 256, 512 and 1024 mJy/beam.

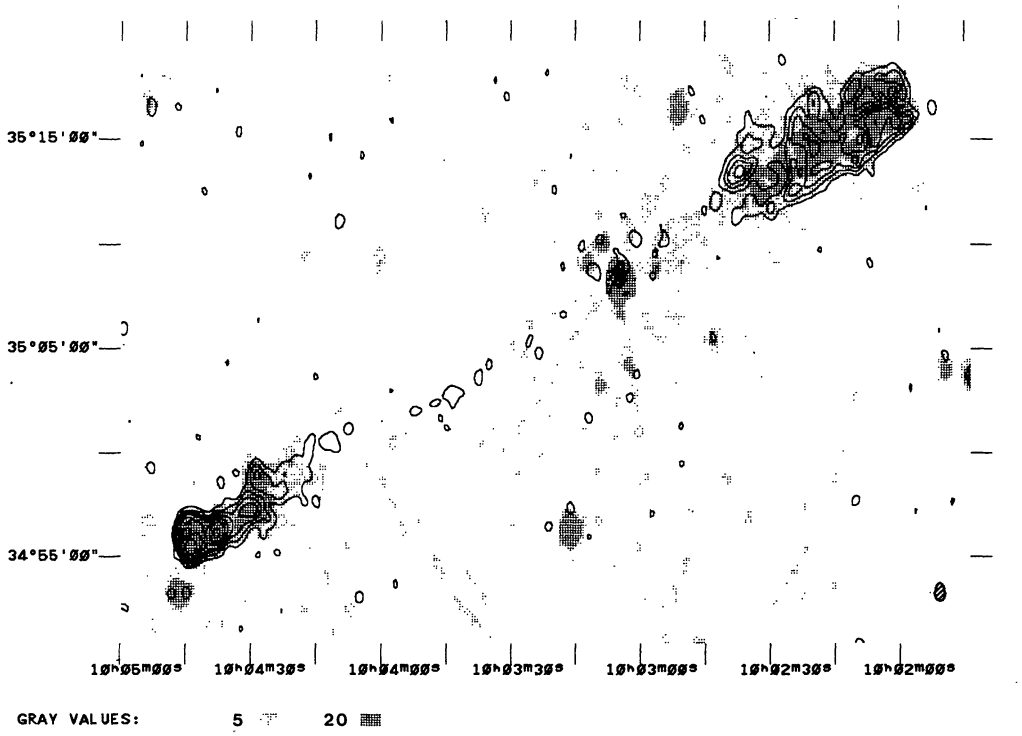

FIGURE 5b. — The linearly polarized intensity distribution of 3C236 at 0.6 GHz. The contour levels are 1.5, 3, 4.5, 6, 9, 12 and 18 mJy/beam.

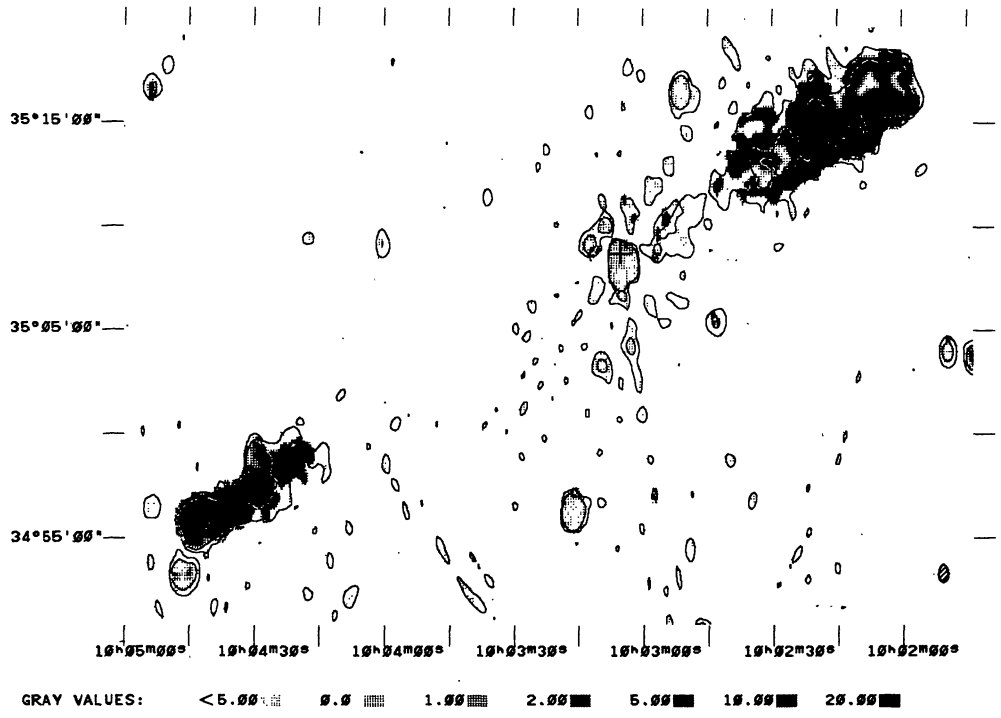

FIGURE 5c. — The distribution of the percentage polarization of 3C236 at 0.6 GHz. The two levels in the total intensity contour map are 5 and 20 mJy/beam.

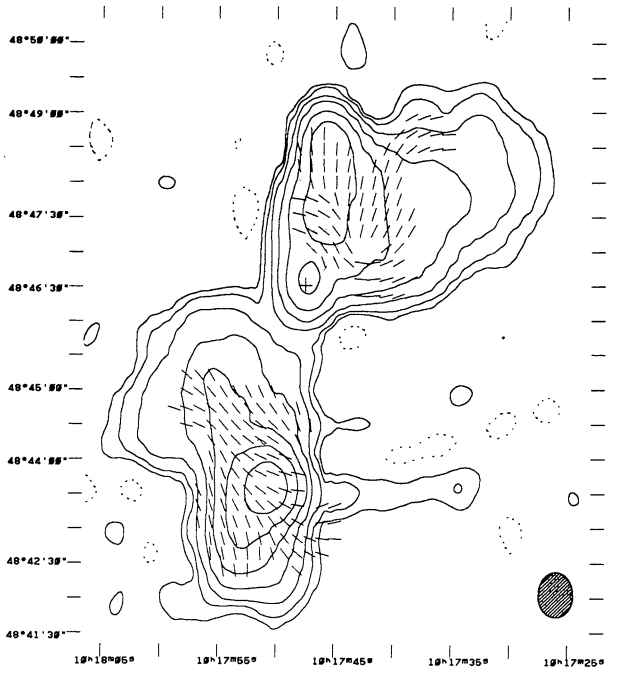

FIGURE 6a. — The total intensity distribution of 4C48.29 at 0.6 GHz. The contour levels are – 4, 4, 8, 16, 32, 64, 128 and 256 mJy/beam.

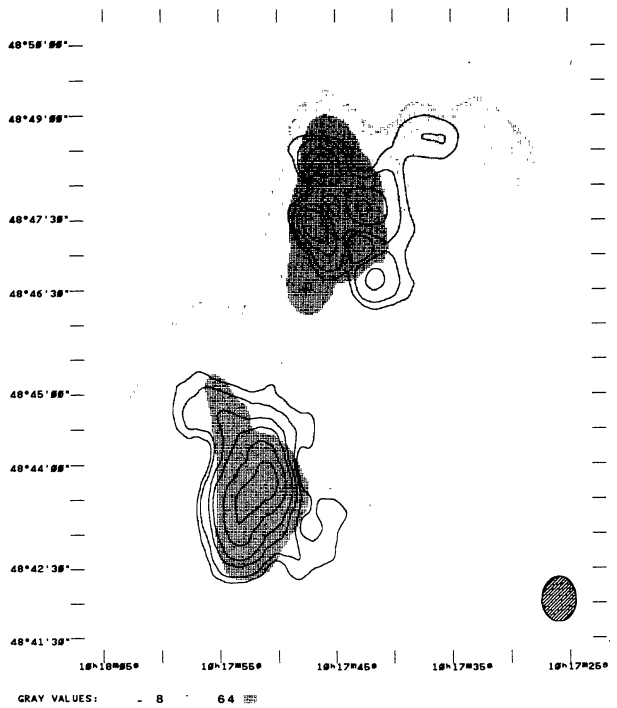

FIGURE 6b. — The linearly polarized intensity distribution of 4C48.29 at 0.6 GHz. The contour levels are 6, 8, 12, 16, 24 and 32 mJy/beam.

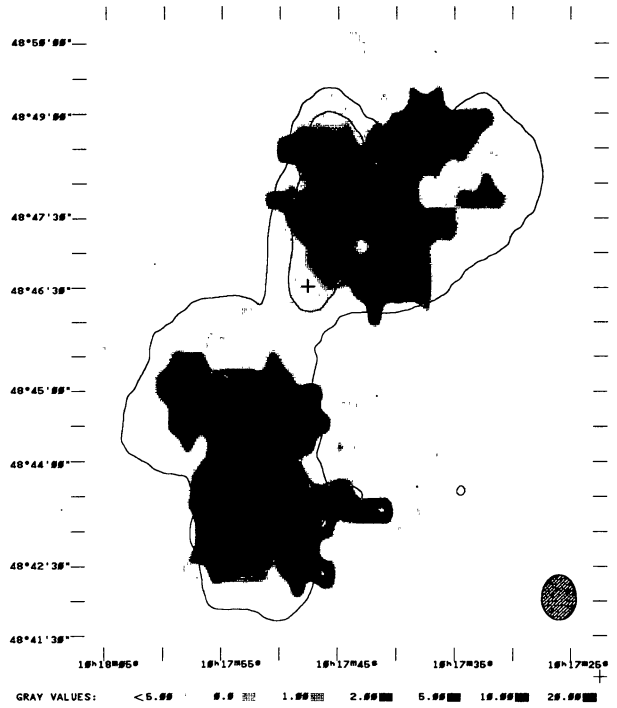

FIGURE 6c. — The distribution of the percentage polarization of 4C48.29 at 0.6 GHz. The two levels in the total intensity contour map are 2 and 64 mJy/beam.

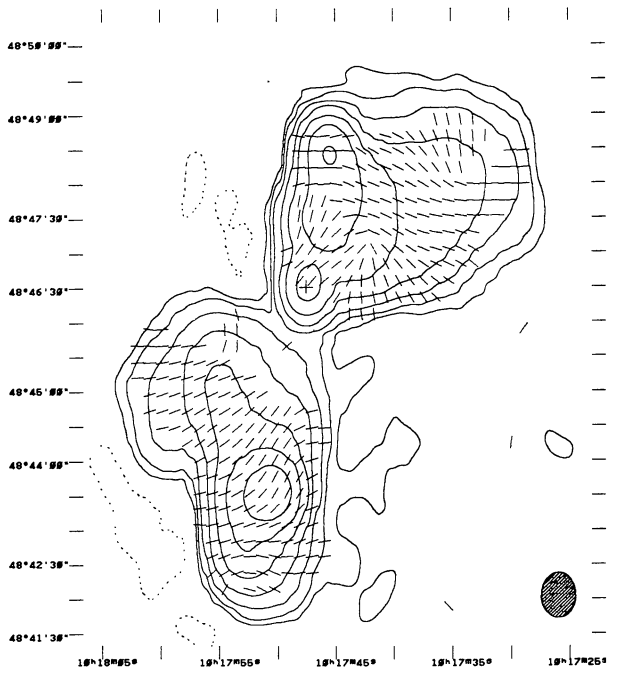

FIGURE 6d. — The total intensity distribution of 4C48.29 at 1.4 GHz. The contour levels are – 2, 2, 4, 8, 16, 32, 64 and 128 mJy/beam.

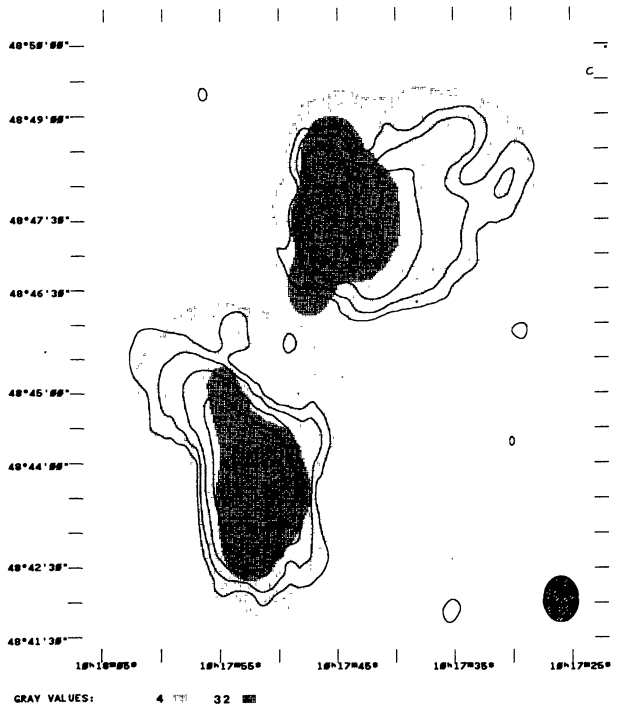

FIGURE 6e. — The linearly polarized intensity distribution of 4C48.29 at 1.4 GHz. The contour levels are 1, 2, 4, 8 and 16 mJy/beam.

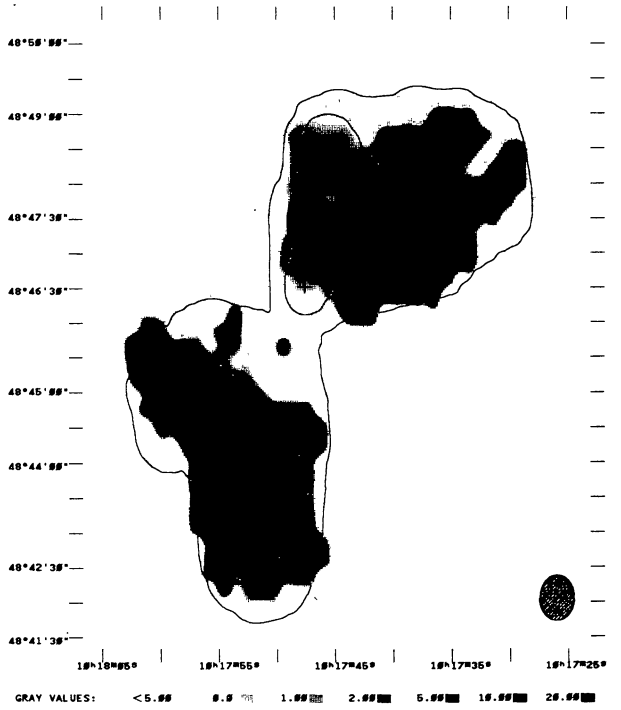

FIGURE 6f. — The distribution of the percentage polarization of 4C48.29 at 1.4 GHz. The two levels in the total intensity contour map are 4 and 32 mJy/beam.

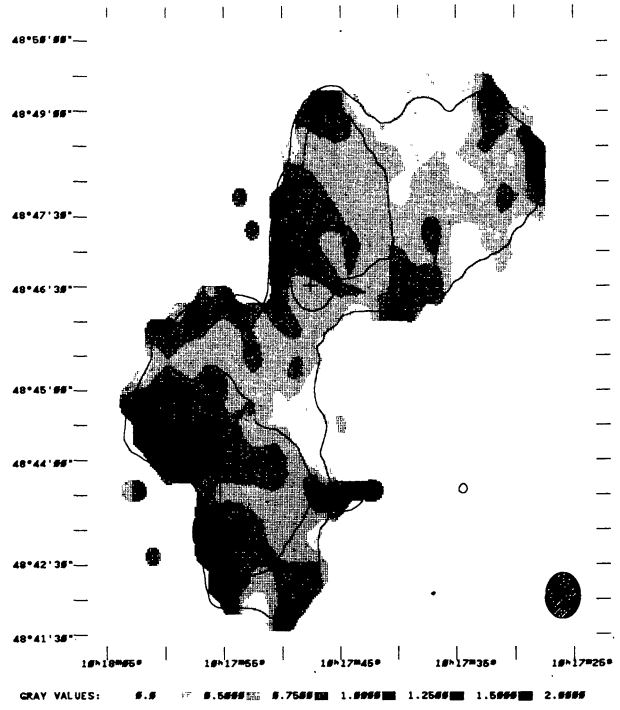

FIGURE 6g. — The distribution of the spectral index of 4C48.29 between 0.6 GHz and 1.4 GHz. The two levels in the total intensity contour map at 0.6 GHz are 8 and 64 mJy/beam.

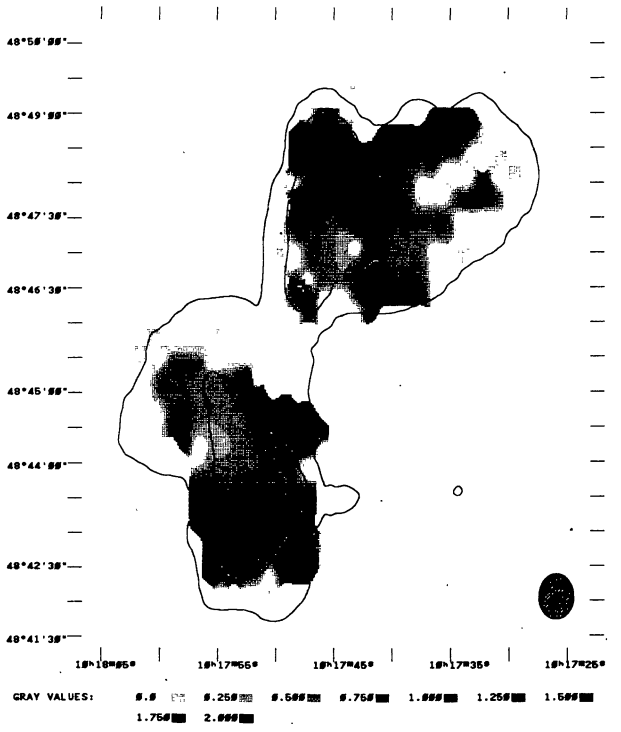

FIGURE 6h. — The distribution of the depolarization of 4C48.29 between 0.6 GHz and 1.4 GHz. The two levels in the total intensity contour map at 0.6 GHz are 8 and 64 mJy/beam.

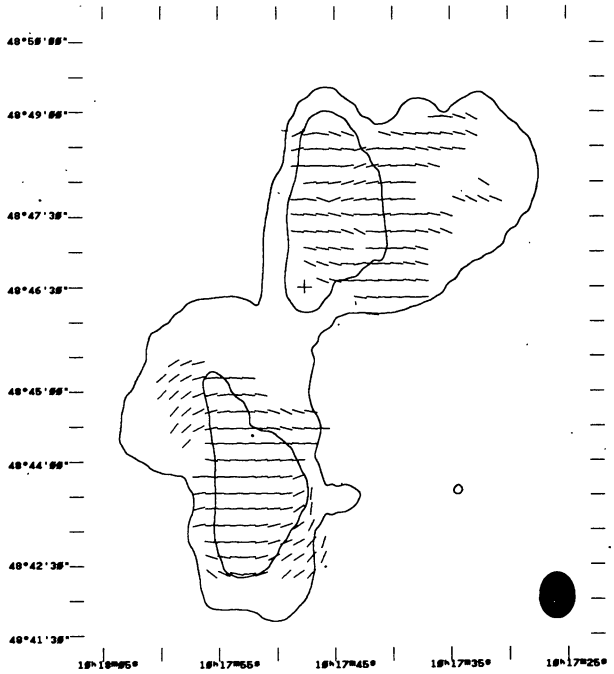

FIGURE 6i. — The distribution of the rotation of the polarization position angle of 4C48.29 between 0.6 GHz and 1.4 GHz measured from the North towards the East. The two levels in the total intensity contour map at 0.6 GHz are 8 and 64 mJy/beam.

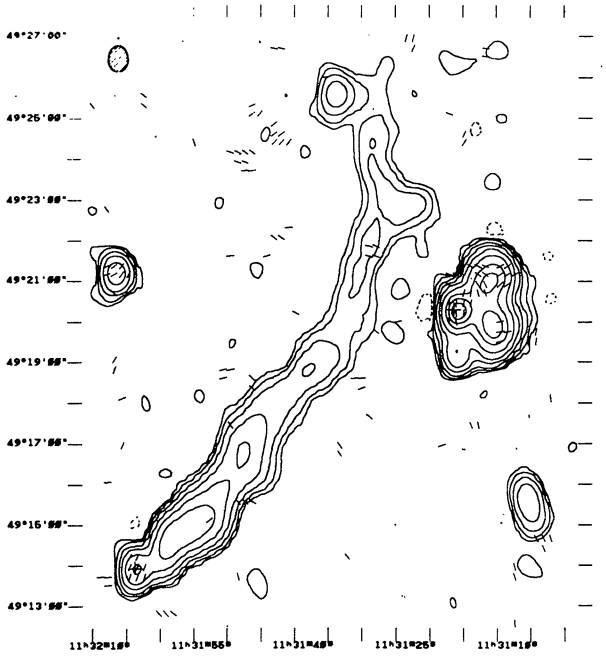

FIGURE 7a. — The total intensity distribution of IC708 & IC711 at 0.6 GHz. The contour levels are – 2, 2, 4, 8, 16, 32, 64, 128, 192 and 256 mJy/beam.

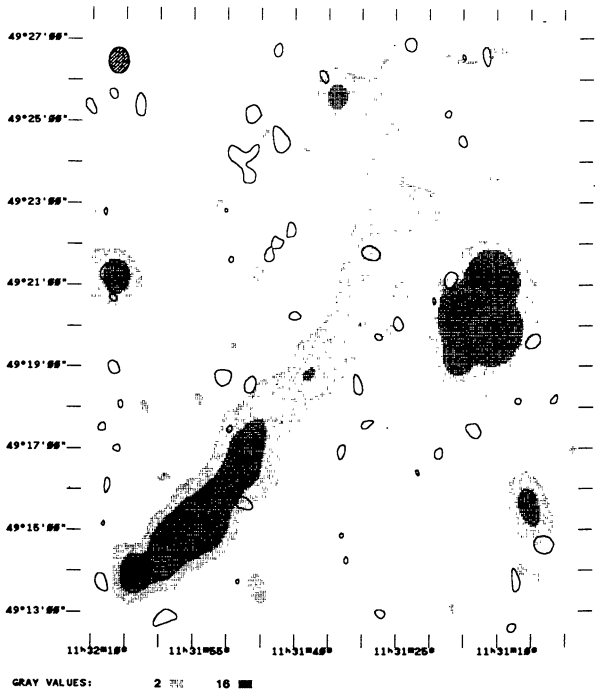

FIGURE 7b. — The linearly polarized intensity distribution of IC708 & IC711 at 0.6 GHz. The contour levels are 1, 1.5 and 2 mJy/beam.

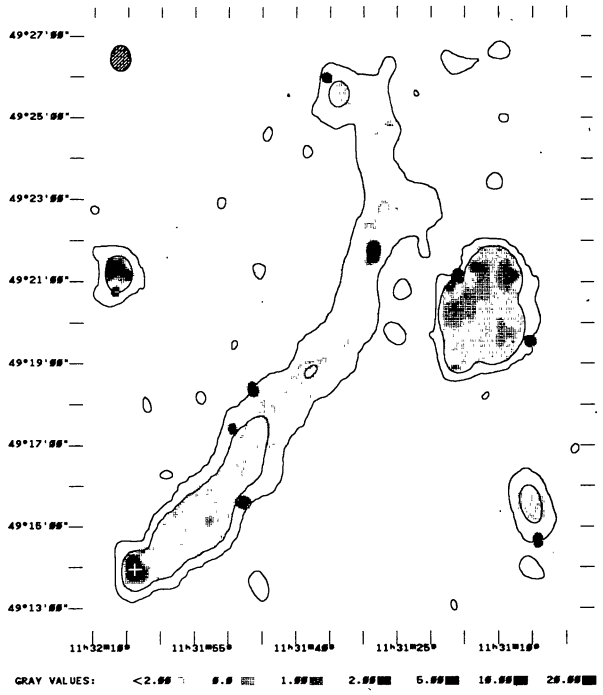

FIGURE 7c. — The distribution of the percentage polarization of IC708 & IC711 at 0.6 GHz. The two levels in the total intensity contour map are 2 and 16 mJy/beam.

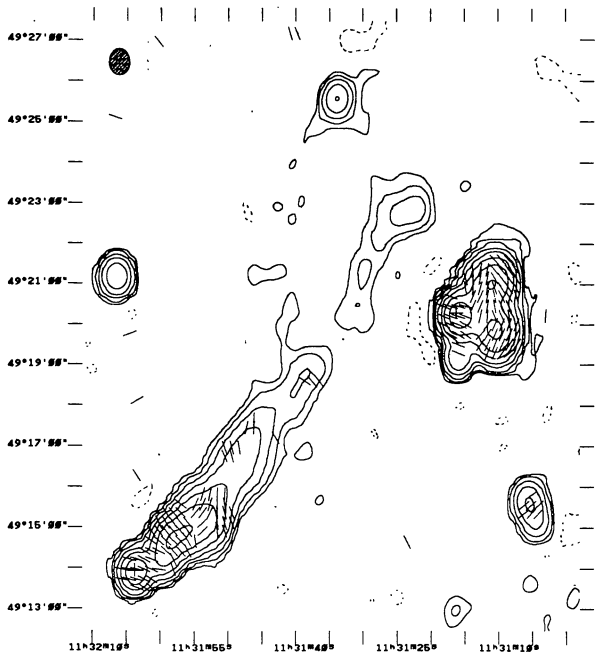

FIGURE 7d. — The total intensity distribution of IC708 & IC711 at 1.4 GHz. The contour levels are – 1, 1, 2, 4, 8, 16, 32, 64 and 128 mJy/beam.

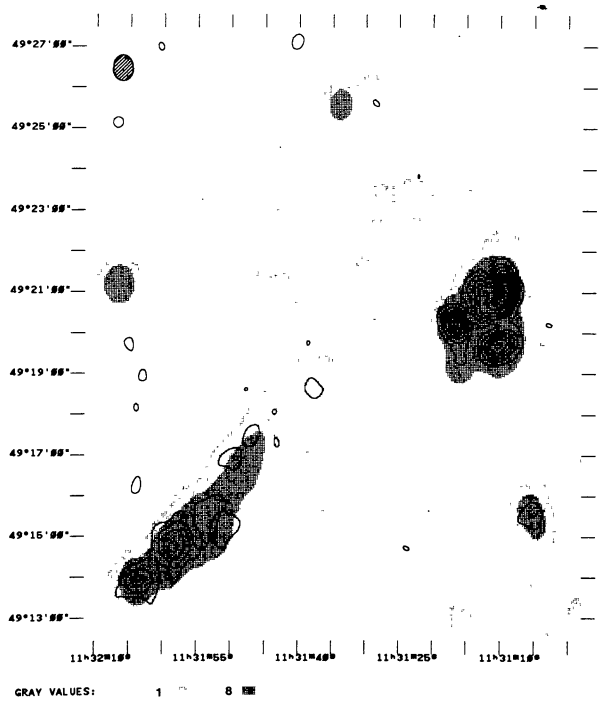

FIGURE 7e. — The linearly polarized intensity distribution of IC708 & IC711 at 1.4 GHz. The contour levels are 0.75, 1.5, 2.25, 3, 3.75, 4.5, 5.25, 6 and 6.75 mJy/beam.

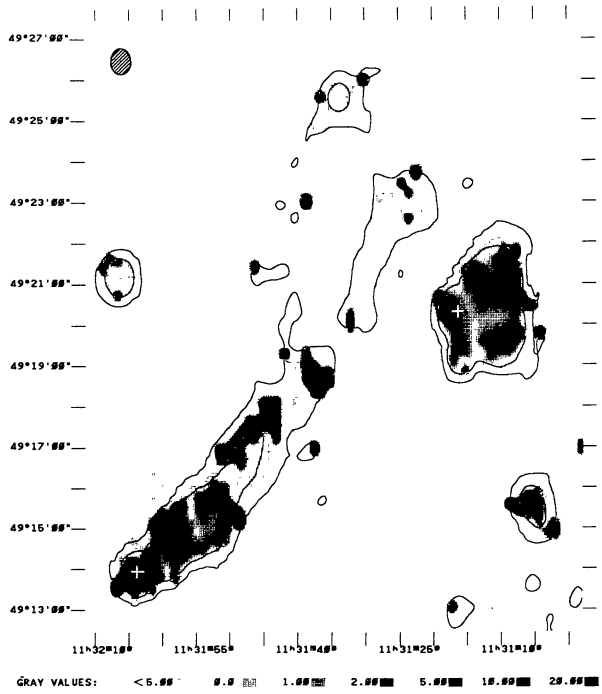

FIGURE 7f. — The distribution of the percentage polarization of IC708 & IC711 at 1.4 GHz. The two levels in the total intensity contour map are 1 and 8 mJy/beam.

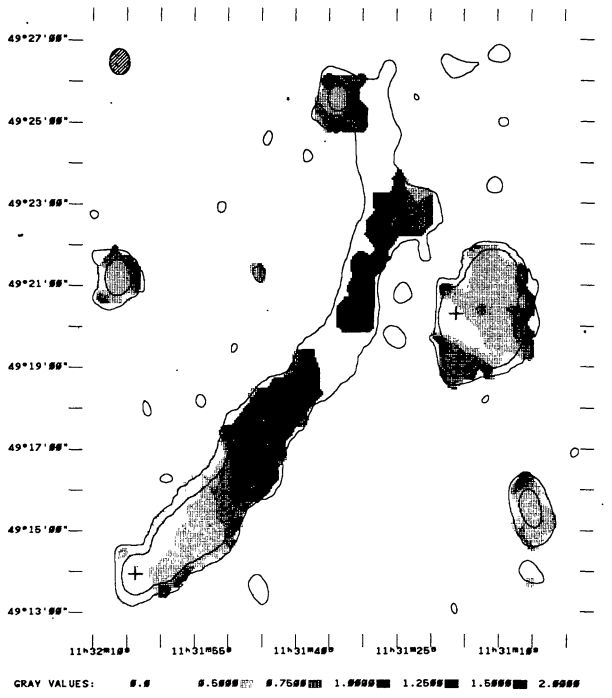

FIGURE 7g. — The distribution of the spectral index of IC708 & IC711 between 0.6 GHz and 1.4 GHz. The two levels in the total intensity contour map at 0.6 GHz are 2 and 16 mJy/beam.

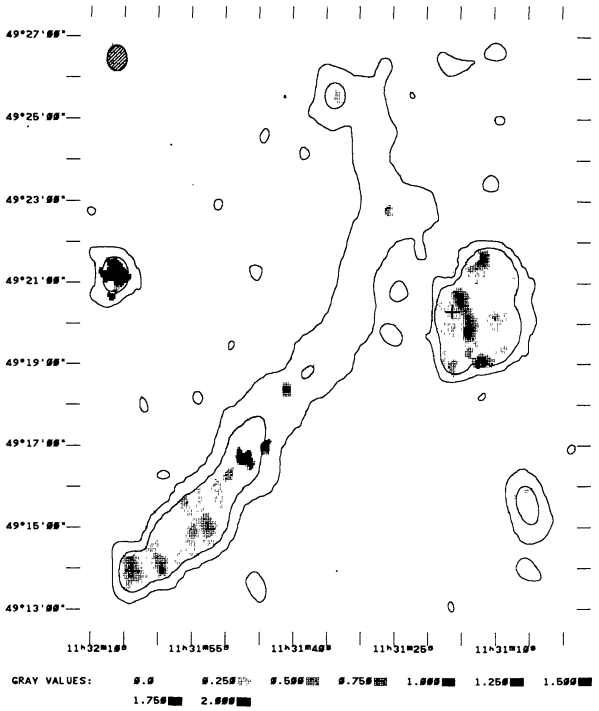

FIGURE 7h. — The distribution of the depolarization of IC708 & IC711 between 0.6 GHz and 1.4 GHz. The two levels in the total intensity contour map at 0.6 GHz are 2 and 16 mJy/beam.

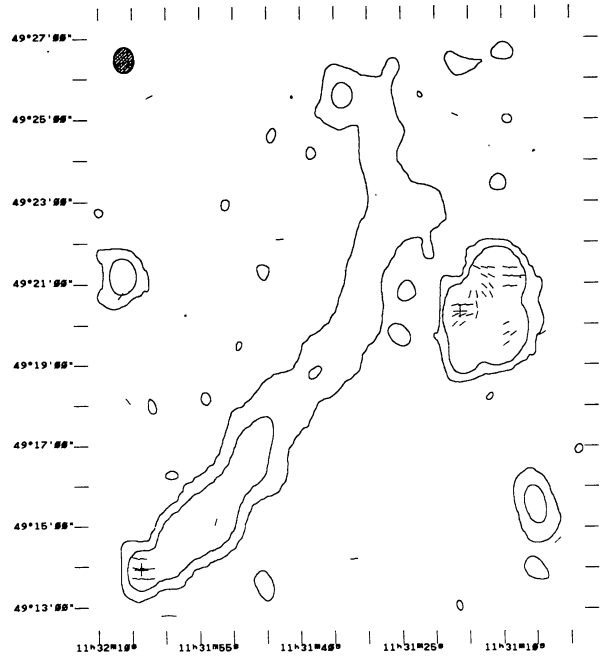

FIGURE 7i. — The distribution of the rotation of the polarization position angle of IC708 & IC711 between 0.6 GHz and 1.4 GHz measured from the North towards the East. The two levels in the total intensity contour map at 0.6 GHz are 2 and 16 mJy/beam.

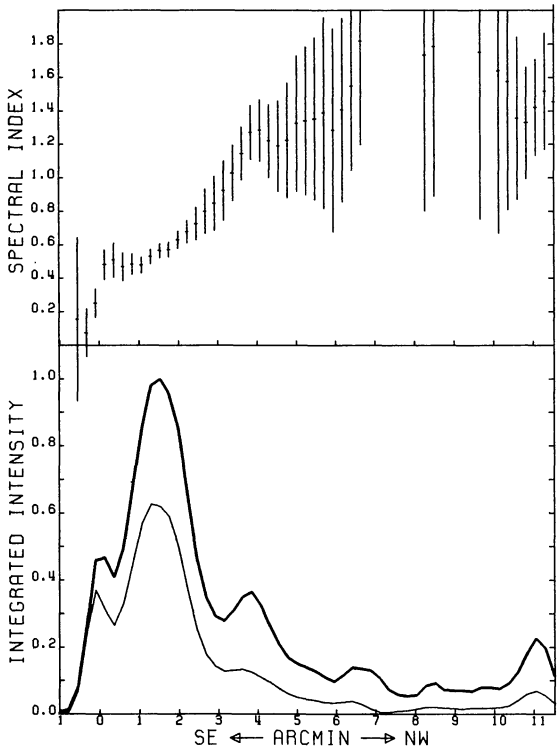

FIGURE 7j. — The spectral index variations along the major axis of IC708 & IC711 between 0.6 GHz and 1.4 GHz. The lower panel shows the (integrated) total intensity along the radio source at 0.6 GHz (thick line) and at 1.4 GHz (thin line). The upper panel shows the variations of the spectral index along the radio source.

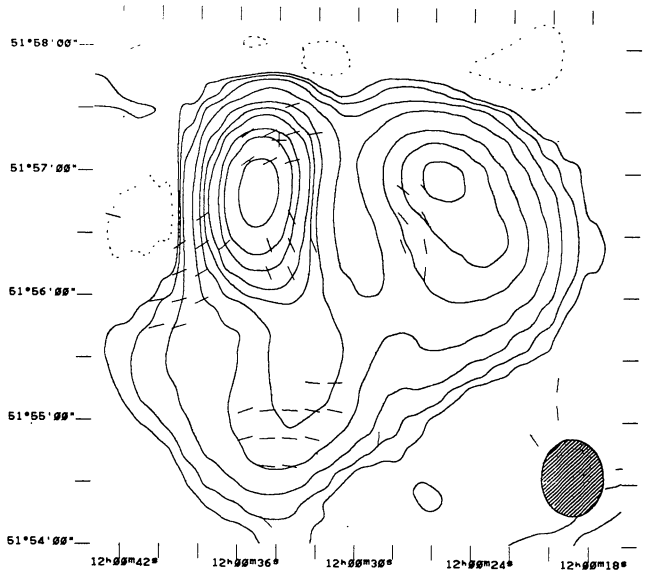

FIGURE 8a. — The total intensity distribution of 4CT51.29.1 at 0.6 GHz. The contour levels are – 2.5, 2.5, 5, 10, 20, 40, 60, 80, 120, 160 and 240 mJy/beam.

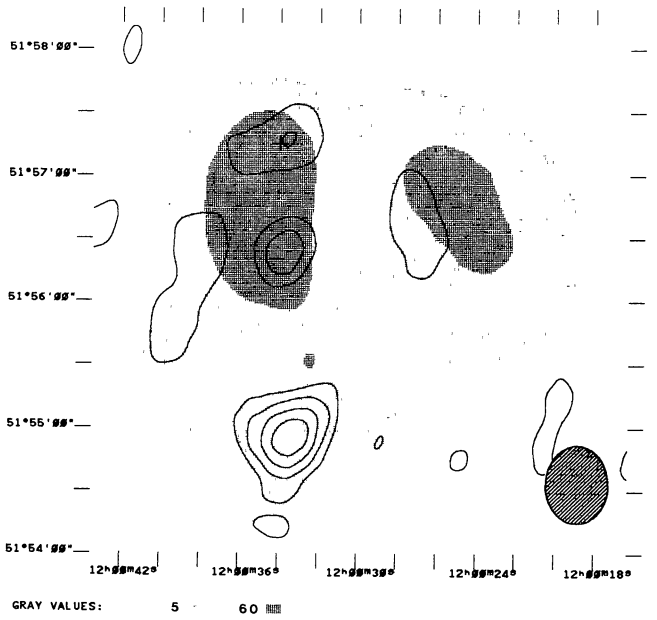

FIGURE 8b. — The linearly polarized intensity distribution of 4CT51.29.1 at 0.6 GHz. The contour levels are 1, 1.5, 2 and 2.5 mJy/beam.

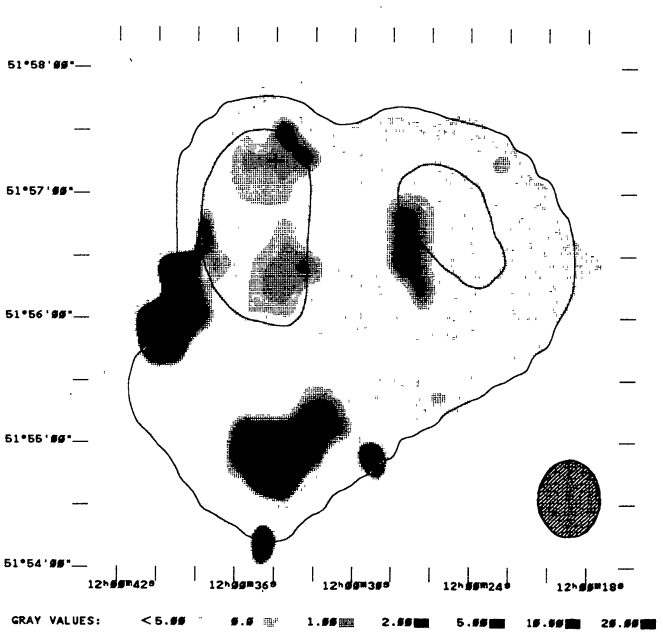

FIGURE 8c. — The distribution of the percentage polarization of 4CT51.29.1 at 0.6 GHz. The two levels in the total intensity contour map are 5 and 60 mJy/beam.

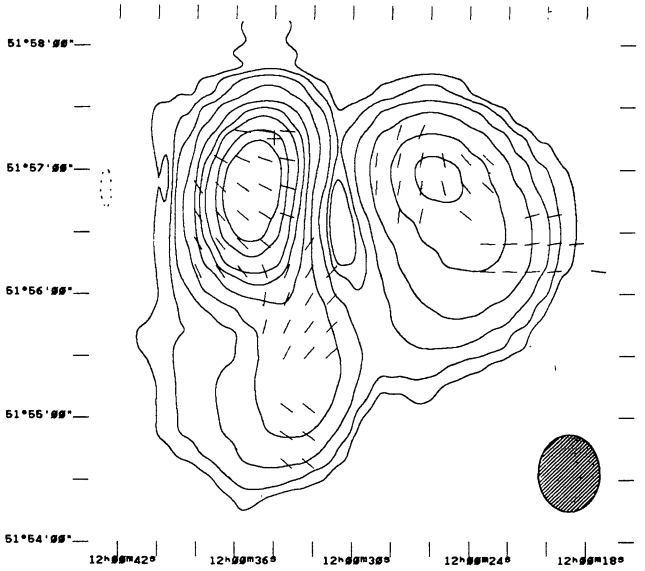

FIGURE 8d. — The total intensity distribution of 4CT51.29.1 at 1.4 GHz. The contour levels are – 2, 2, 4, 8, 16, 32, 48, 64, 96 and 128 mJy/beam.

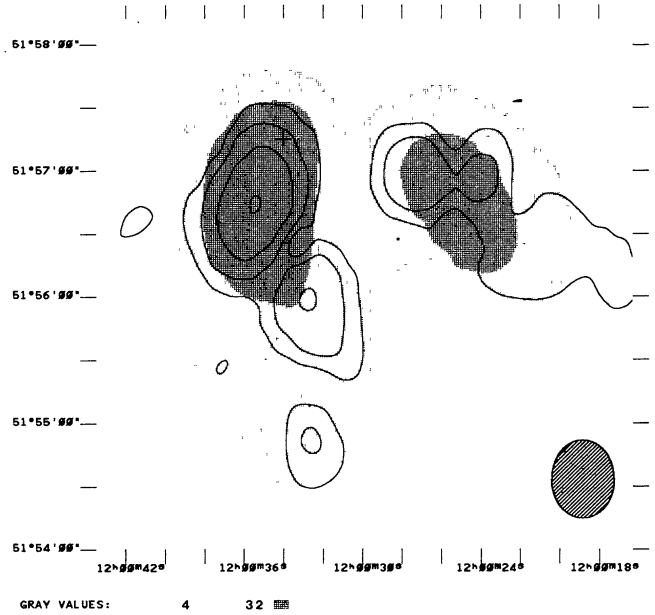

FIGURE 8e. — The linearly polarized intensity distribution of 4CT51.29.1 at 1.4 GHz. The contour levels are 1.25, 2.5, 5 and 10 mJy/beam.

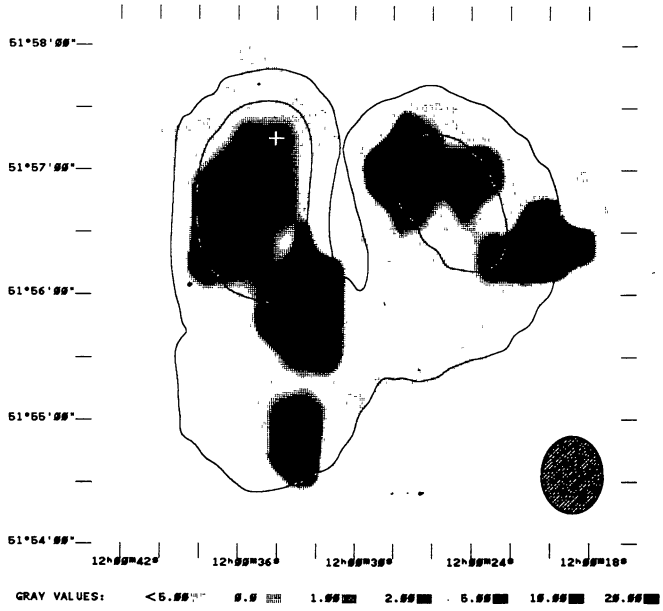

FIGURE 8f. — The distribution of the percentage polarization of 4CT51.29.1 at 1.4 GHz. The two levels in the total intensity contour map are 4 and 32 mJy/beam.

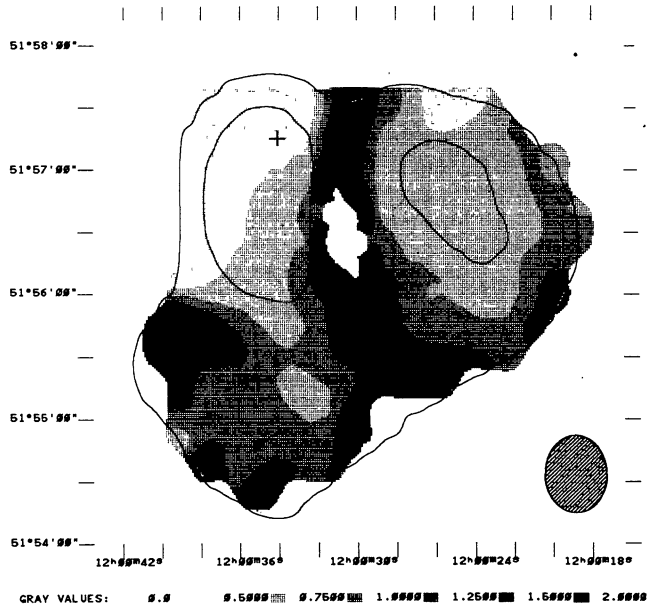

FIGURE 8g. — The distribution of the spectral index of 4CT51.29.1 between 0.6 GHz and 1.4 GHz. The two levels in the total intensity contour map at 0.6 GHz are 5 and 60 mJy/beam.

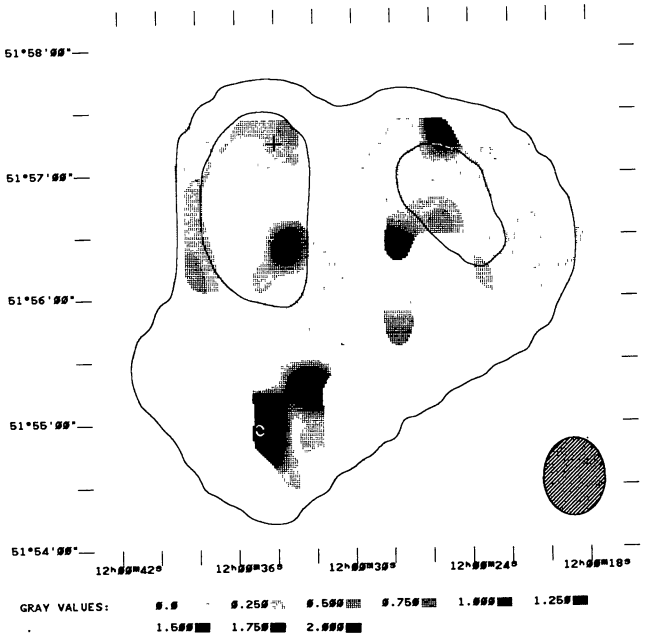

FIGURE 8h. — The distribution of the depolarization of 4CT51.29.1 between 0.6 GHz and 1.4 GHz. The two levels in the total intensity contour map at 0.6 GHz are 5 and 60 mJy/beam.

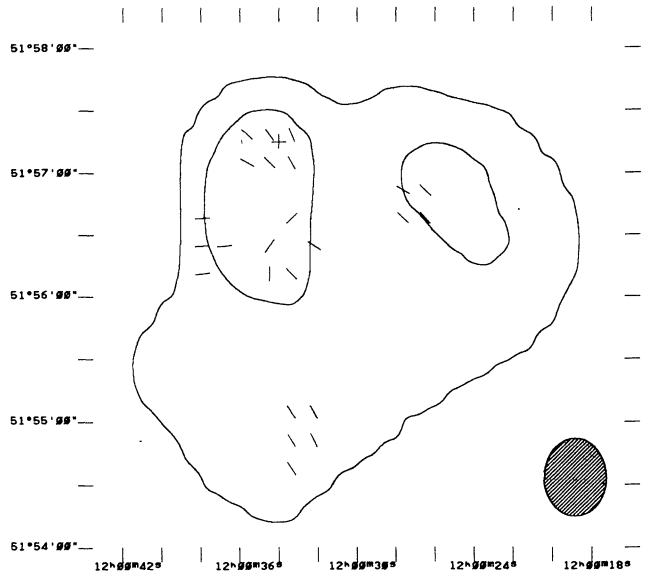

FIGURE 8i. — The distribution of the rotation of the polarization position angle of 4CT51.29.1 between 0.6 GHz and 1.4 GHz measured from the North towards the East. The two levels in the total intensity contour map at 0.6 GHz are 5 and 60 mJy/beam.

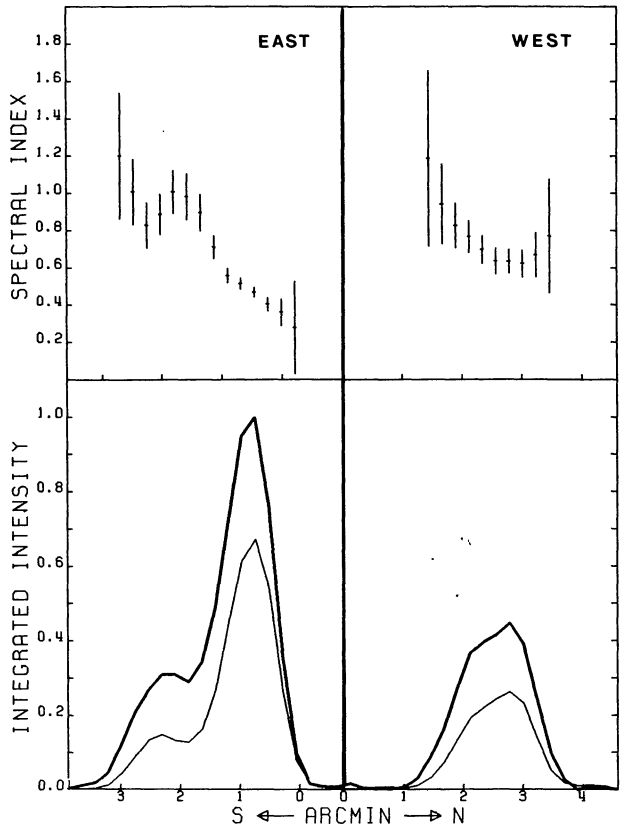

FIGURE 8j. — The spectral index variations along the major axis of 4CT51.29.1 between 0.6 GHz and 1.4 GHz. The lower panel shows the (integrated) total intensity along the radio source at 0.6 GHz (thick line) and at 1.4 GHz (thin line). The upper panel shows the variations of the spectral index along the radio source.

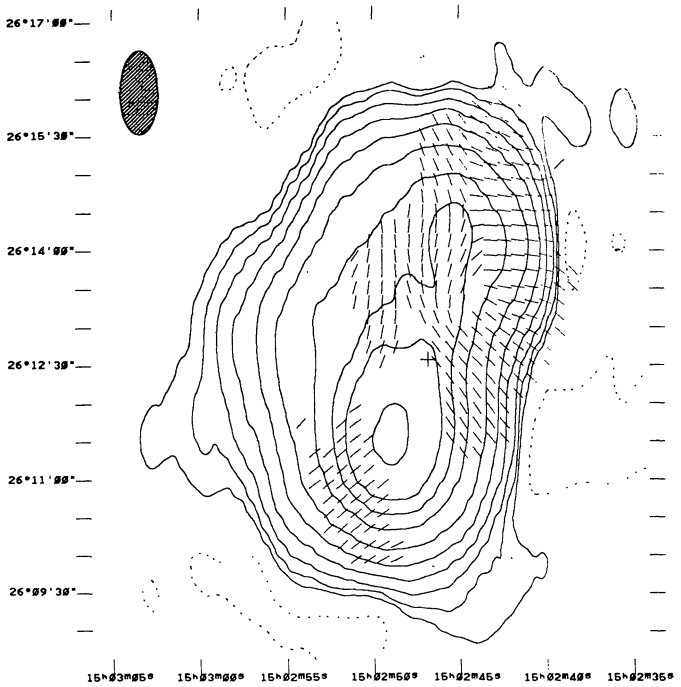

FIGURE 9a. — The total intensity distribution of 3C310 at 0.6 GHz. The contour levels are – 10, 10, 20, 40, 80, 160, 320, 640, 960, 1280 and 1920 mJy/beam.

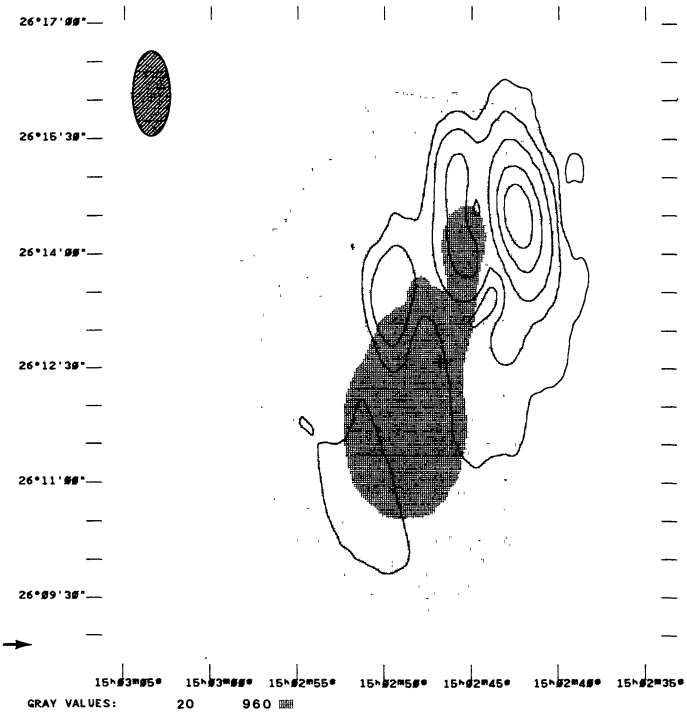

FIGURE 9b. — The linearly polarized intensity distribution of 3C310 at 0.6 GHz. The contour levels are 5, 10, 20, 40 and 60 mJy/beam.

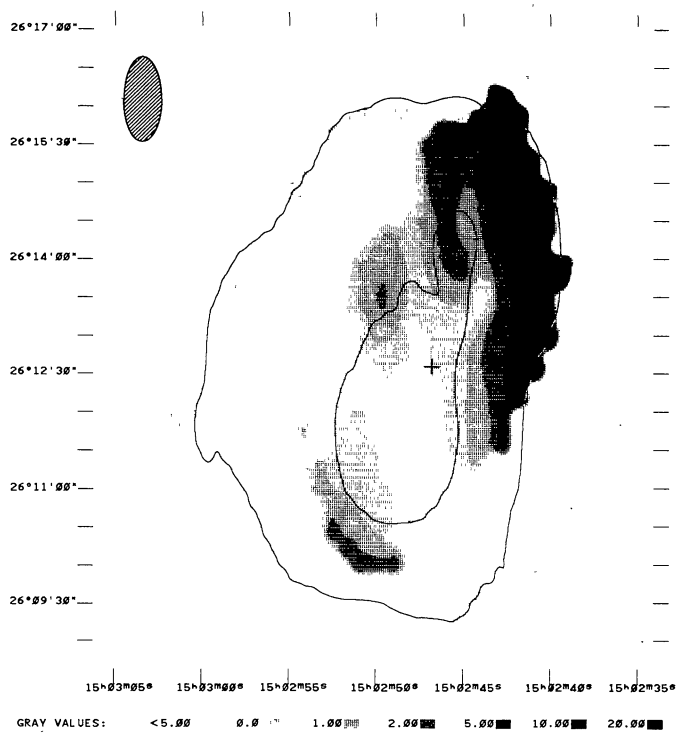

FIGURE 9c. — The distribution of the percentage polarization of 3C310 at 0.6 GHz. The two levels in the total intensity contour map are 20 and 960 mJy/beam.

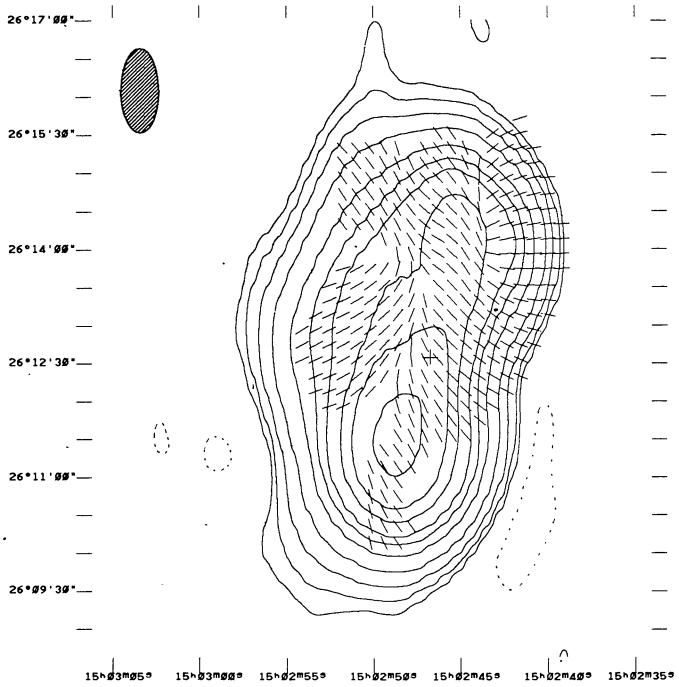

FIGURE 9d. — The total intensity distribution of 3C310 at 1.4 GHz. The contour levels are – 7.5, 7.5, 15, 30, 60, 120, 180, 240, 360, 480 and 720 mJy/beam.

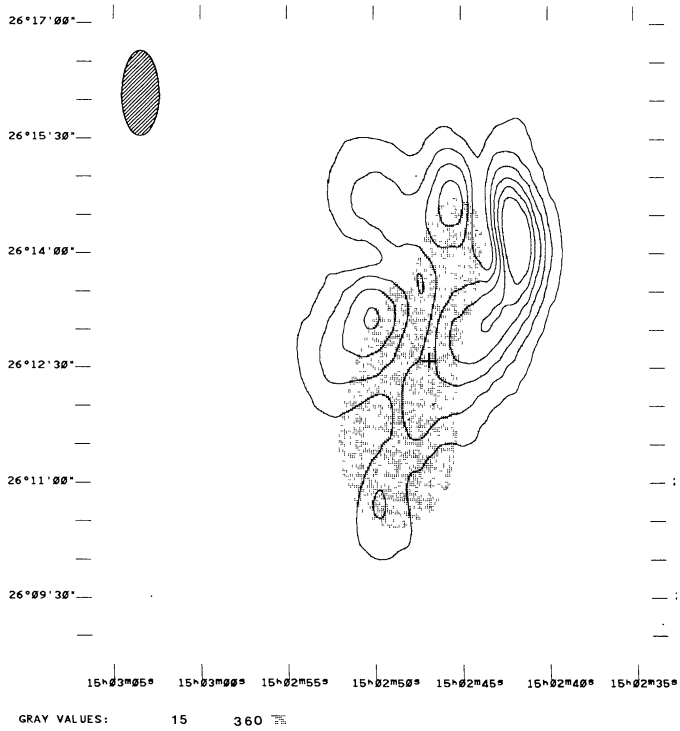

FIGURE 9e. — The linearly polarized intensity distribution of 3C310 at 1.4 GHz. The contour levels are 7.5, 15, 22.5, 30, 37.5 and 45 mJy/beam.

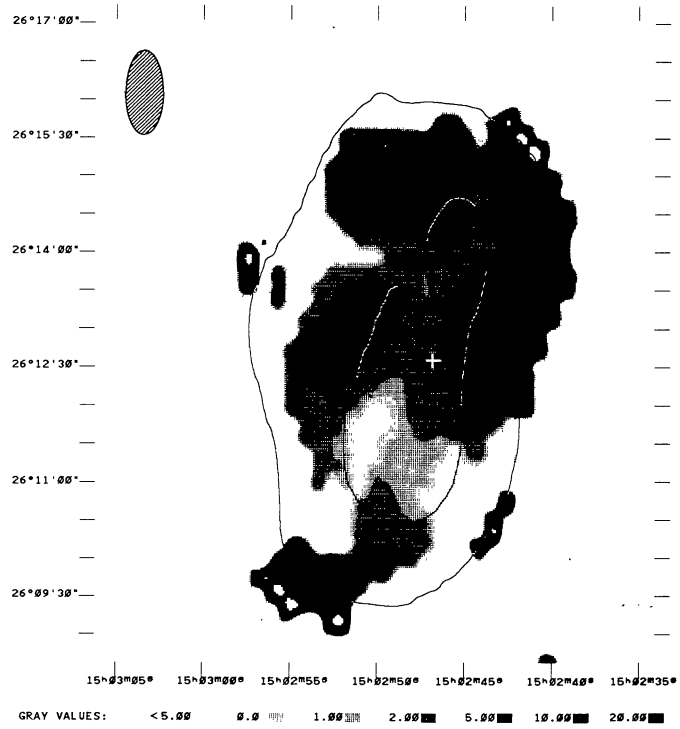

FIGURE 9f. — The distribution of the percentage polarization of 3C310 at 1.4 GHz. The two levels in the total intensity contour map are 15 and 360 mJy/beam.

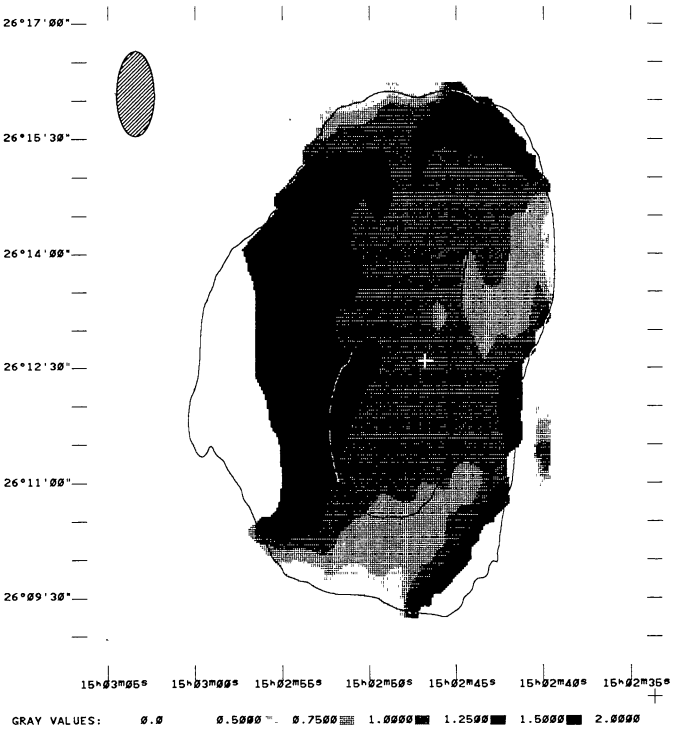

FIGURE 9g. — The distribution of the spectral index of 3C310 between 0.6 GHz and 1.4 GHz. The two levels in the total intensity contour map at 0.6 GHz are 20 and 960 mJy/beam.

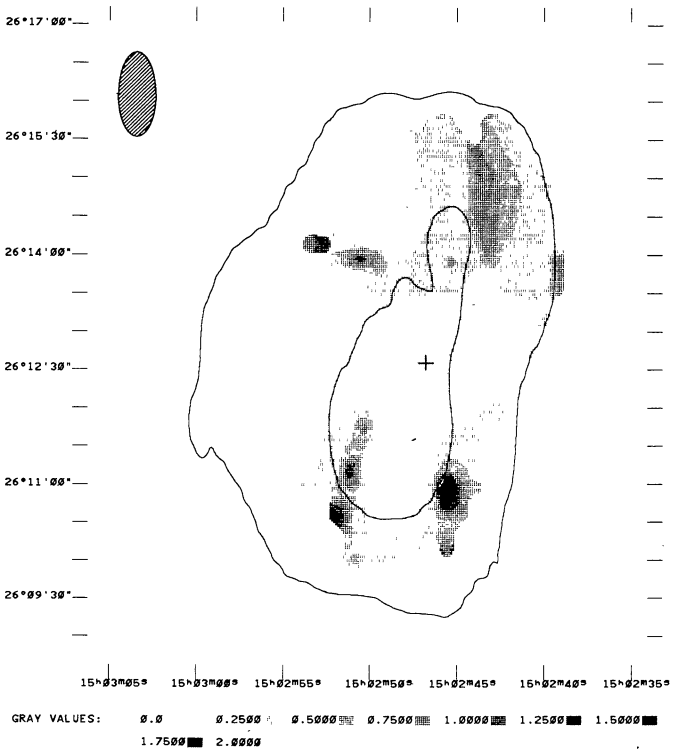

FIGURE 9h. — The distribution of the depolarization of 3C310 between 0.6 GHz and 1.4 GHz. The two levels in the total intensity contour map at 0.6 GHz are 20 and 960 mJy/beam.

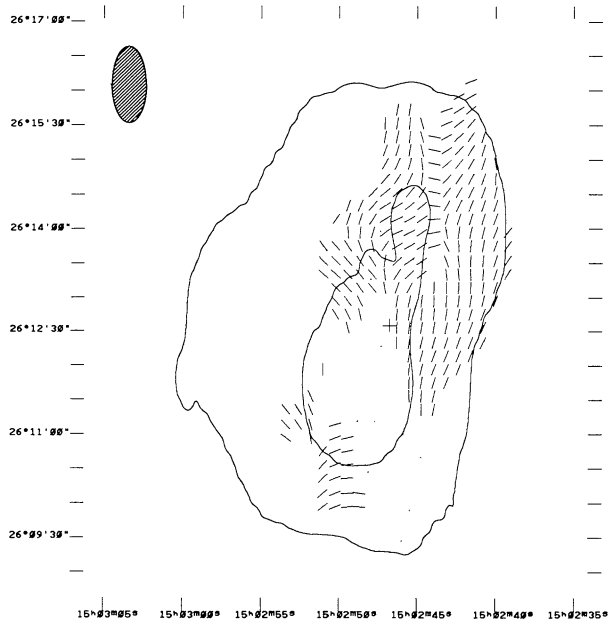

FIGURE 9i. — The distribution of the rotation of the polarization position angle of 3C310 between 0.6 GHz and 1.4 GHz measured from the North towards the East. The two levels in the total intensity contour map at 0.6 GHz are 20 and 960 mJy/beam.

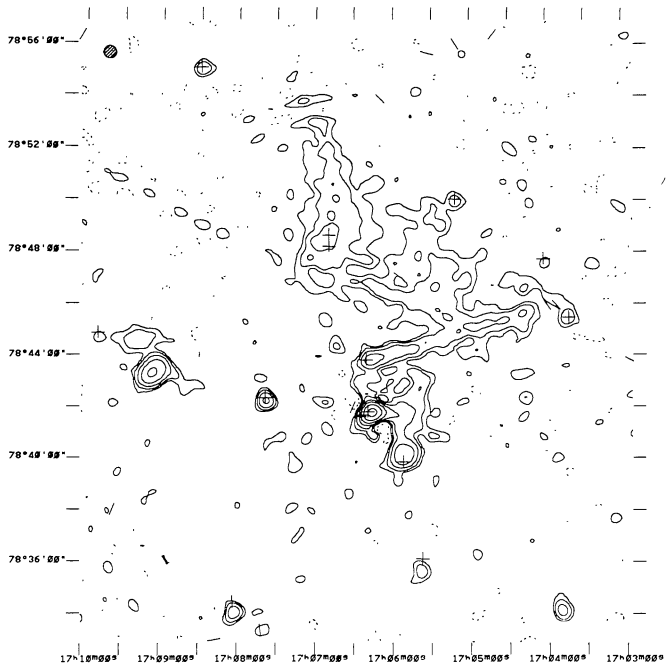

FIGURE 10a. — The total intensity distribution of Abell2256 at 0.6 GHz. The contour levels are – 2.5, 2.5, 5, 10, 20, 40, 80 and 160 mJy/beam.

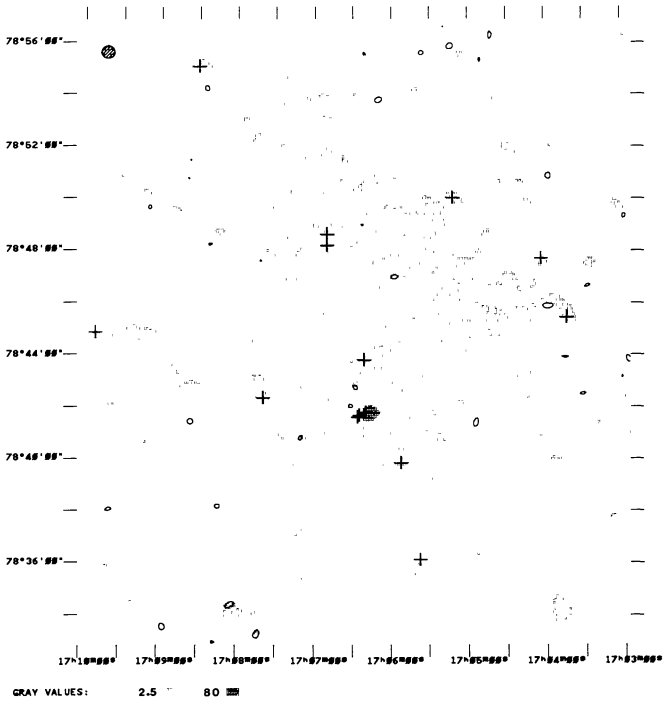

FIGURE 10b. — The linearly polarized intensity distribution of Abell2256 at 0.6 GHz. The contour level is 2 mJy/beam.

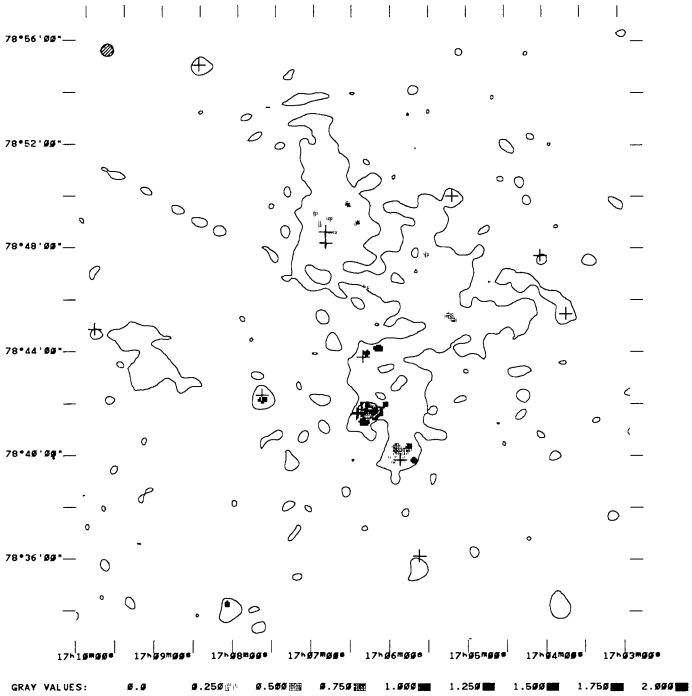

FIGURE 10c. — The distribution of the percentage polarization of Abell2256 at 0.6 GHz. The two levels in the total intensity contour map are 2.5 and 80 mJy/beam.

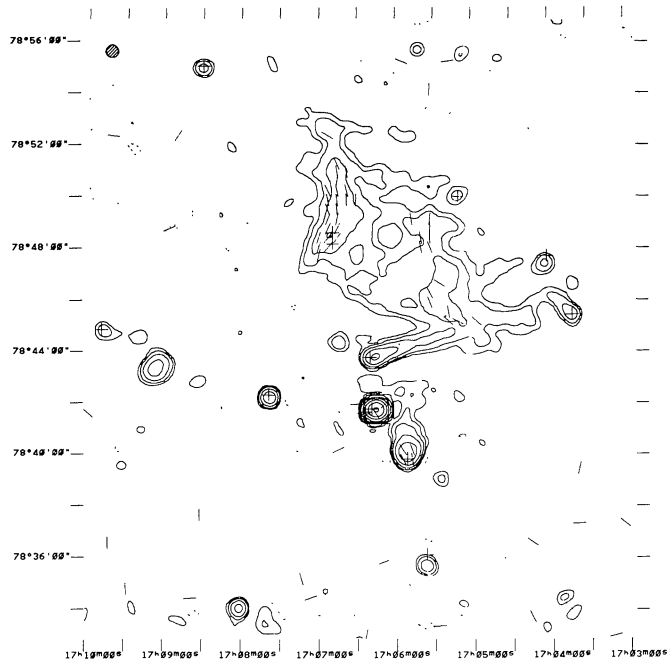

FIGURE 10d. — The total intensity distribution of Abell2256 at 1.4 GHz. The contour levels are – 0.75, 0.75, 1.5, 3, 6, 12, 24, 48 and 96 mJy/beam.

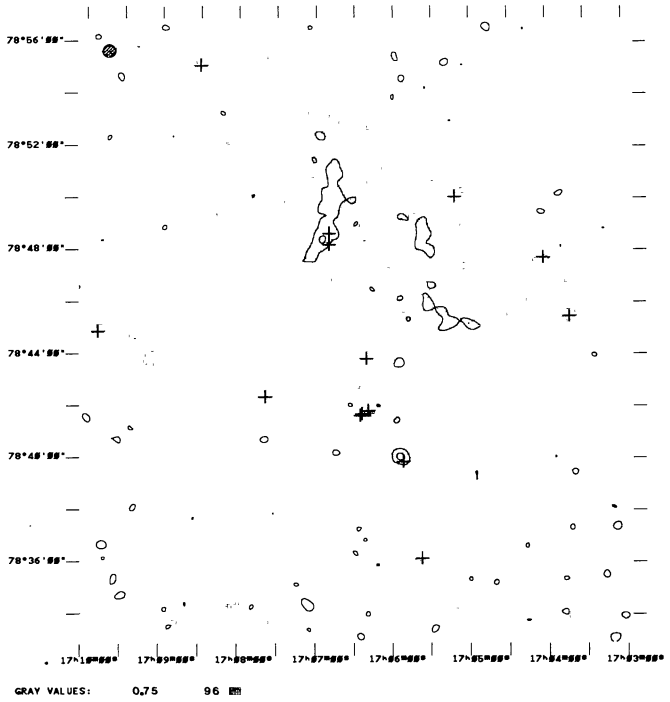

FIGURE 10e. — The linearly polarized intensity distribution of Abell2256 at 1.4 GHz. The contour levels are 0.75 and 1.5 mJy/beam.

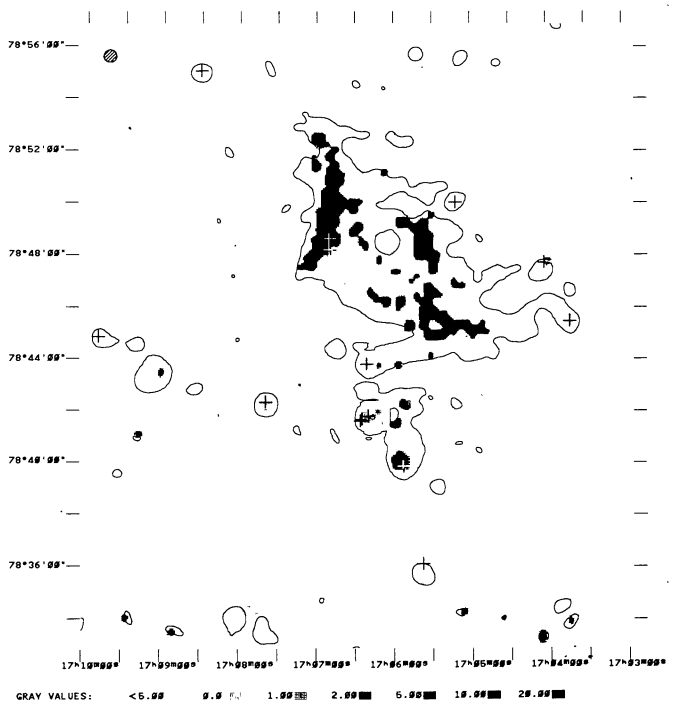

FIGURE 10f. — The distribution of percentage polarization of Abell2256 at 1.4 GHz. The two levels in the total intensity contour map are 0.75 and 96 mJy/beam.

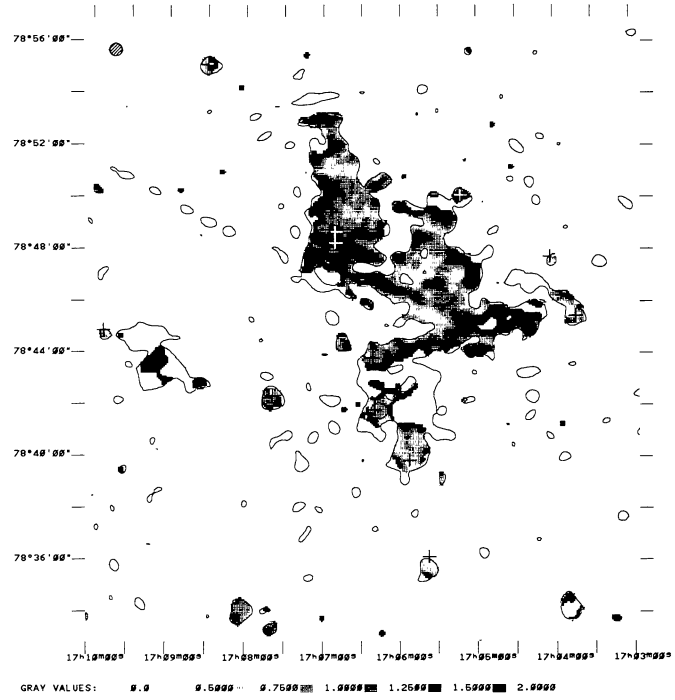

FIGURE 10g. — The distribution of the spectral index of Abell2256 between 0.6 GHz and 1.4 GHz. The two levels in the total intensity contour map at 0.6 GHz are 2.5 and 80 mJy/beam.

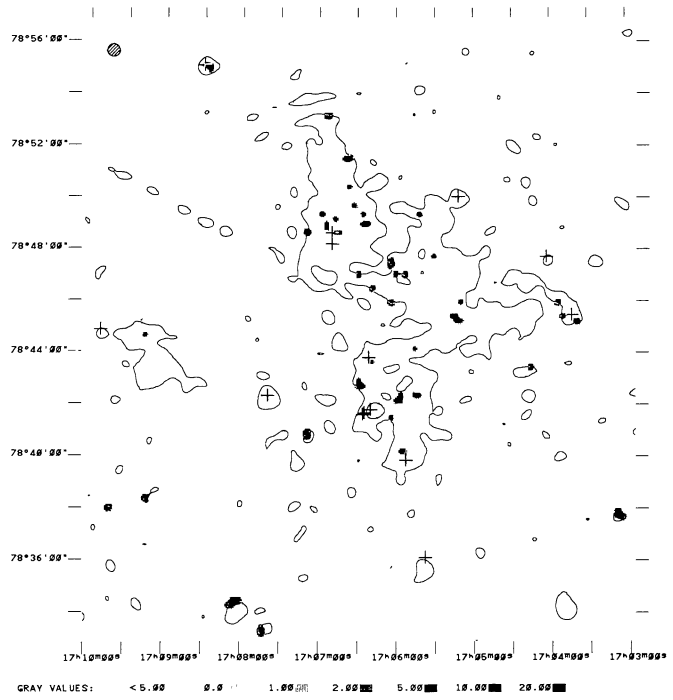

FIGURE 10h. — The distribution of the depolarization of Abell2256 between 0.6 GHz and 1.4 GHz. The two levels in the total intensity contour map at 0.6 GHz are 2.5 and 80 mJy/beam.

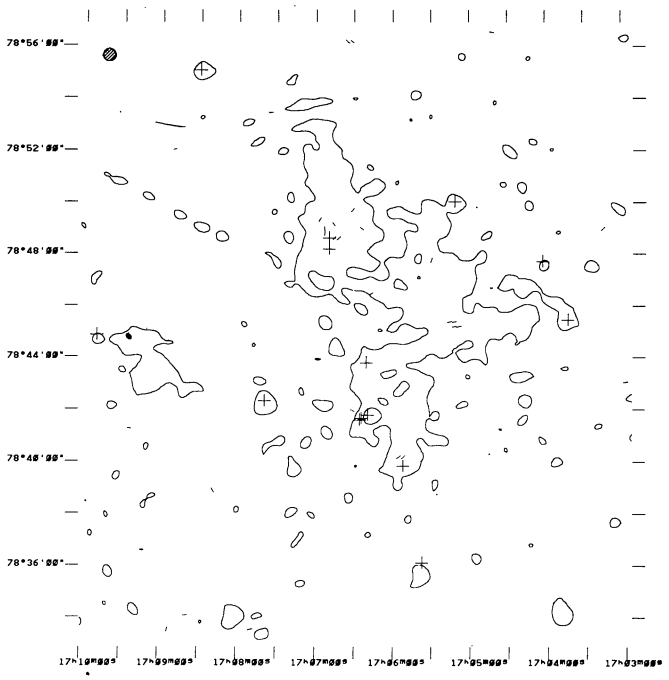

FIGURE 10i. — The distribution of the rotation of the polarization position angle of 3CC33.1 between 0.6 GHz and 1.4 GHz measured from the North towards the East. The two levels in the total intensity contour map at 0.6 GHz are 2.5 and 80 mJy/beam.

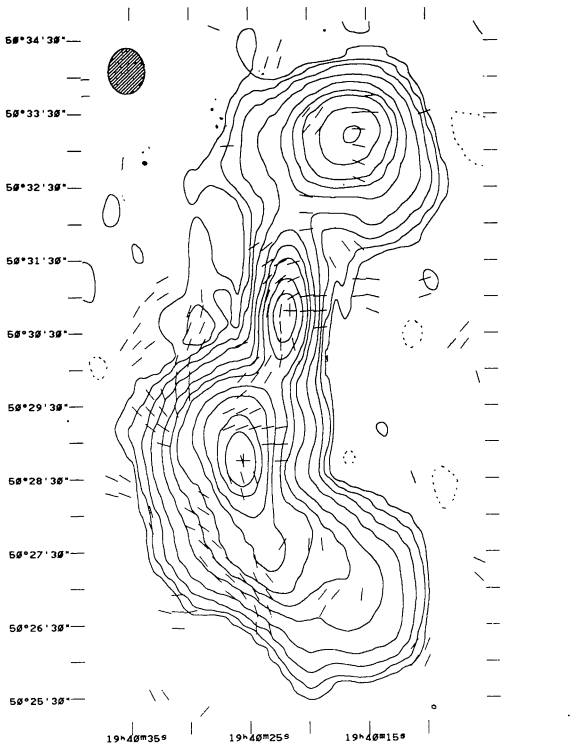

FIGURE 11a. — The total intensity distribution of 3C402 at 0.6 GHz. The contour levels are – 4, 4, 8, 16, 32, 64, 96, 128, 192, 256, 384 and 512 mJy/beam.

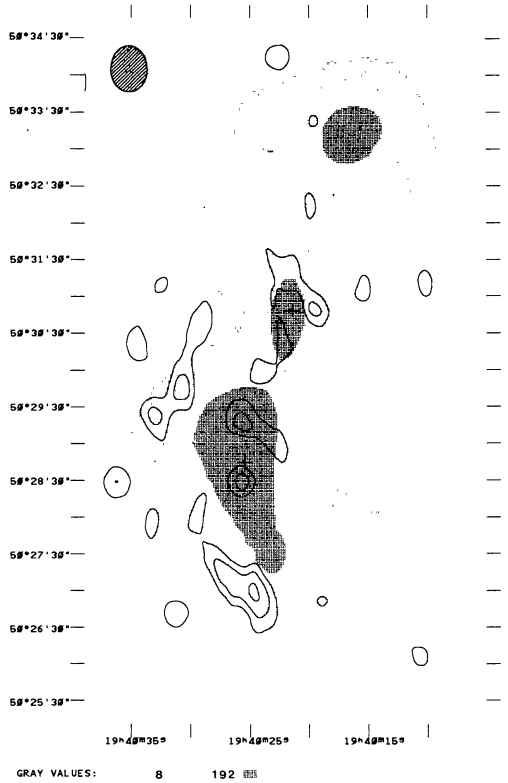

FIGURE 11b. — The linearly polarized intensity distribution of 3C402 at 0.6 Ghz. The contour levels are 3, 4 and 5 mJy/beam.

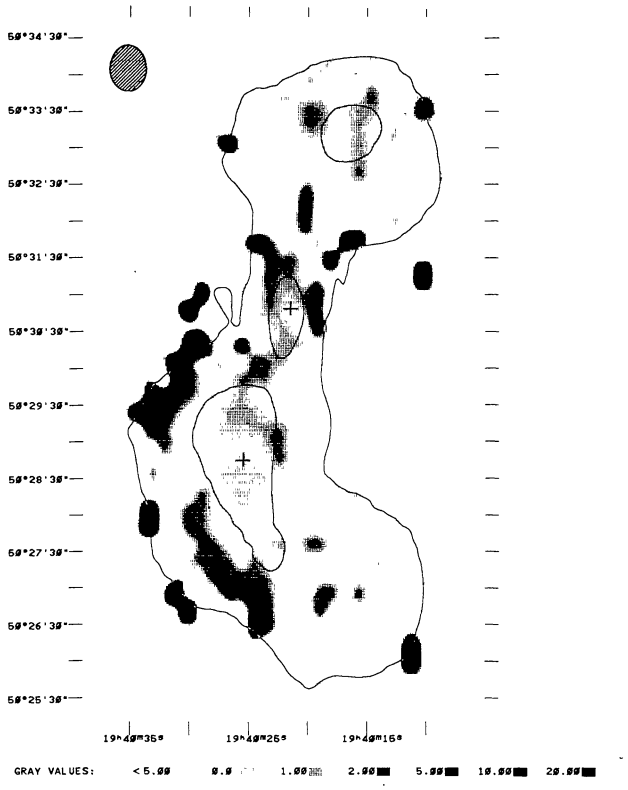

FIGURE 11c. — The distribution of the percentage polarization of 3C402 at 0.6 GHz. The two levels in the total intensity contour map are 8 and 192 mJy/beam.

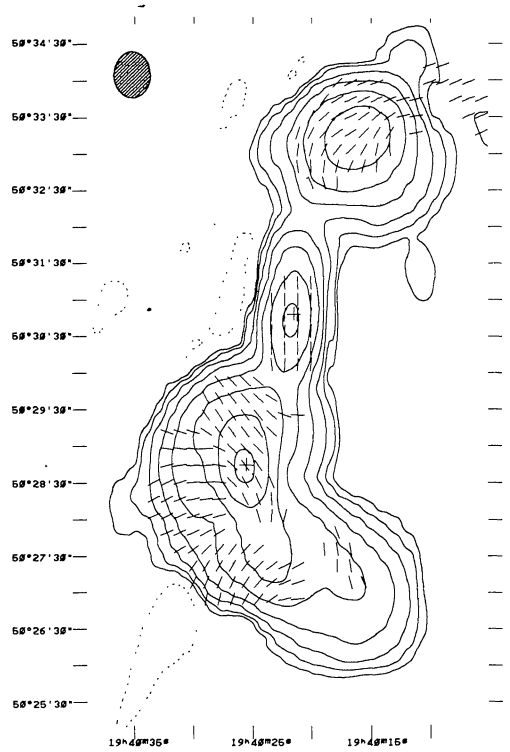

FIGURE 11d. — The total intensity distribution of 3C402 at 1.4 GHz. The contour levels are – 3, 3, 6, 12, 24, 48, 96, 192 and 384 mJybeam.

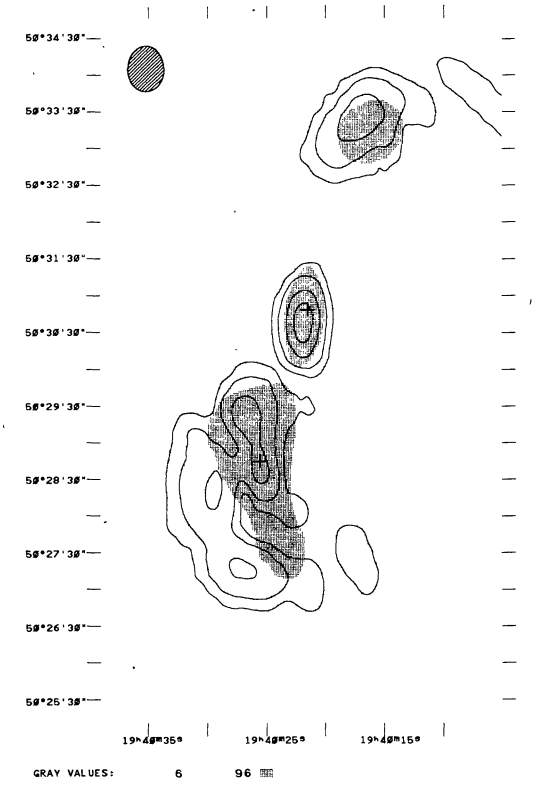

FIGURE 11e. — The linearly polarized intensity distribution of 3C402 at 1.4 GHz. The contour levels are 2.5, 5, 10 and 15 mJy/beam.

FIGURE 11f. — The distribution of the percentage polarization of 3C402 at 1.4 GHz. The two levels in the total intensity contour map are 6 and 96 mJy/beam.

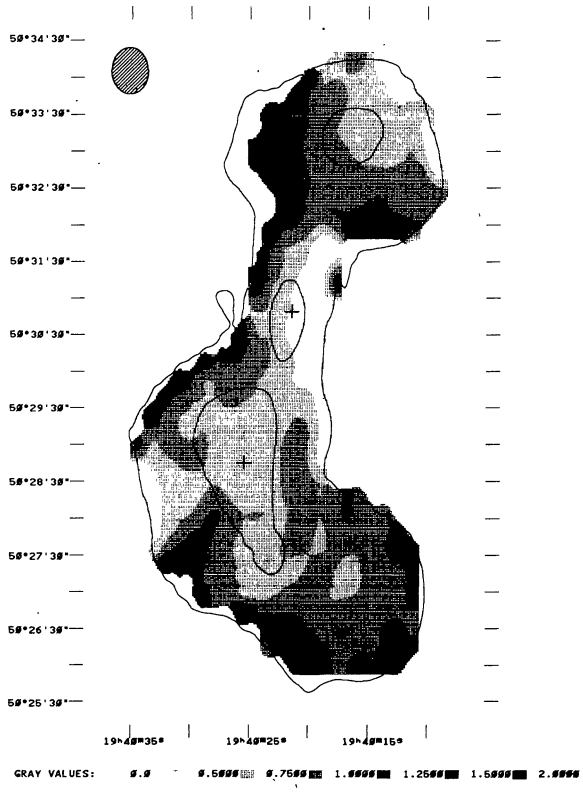

FIGURE 11g. — The distribution of the spectral index of 3C402 between 0.6 GHz and 1.4 GHz. The two levels in the total intensity contour map at 0.6 GHz are 8 and 192 mJy/beam.

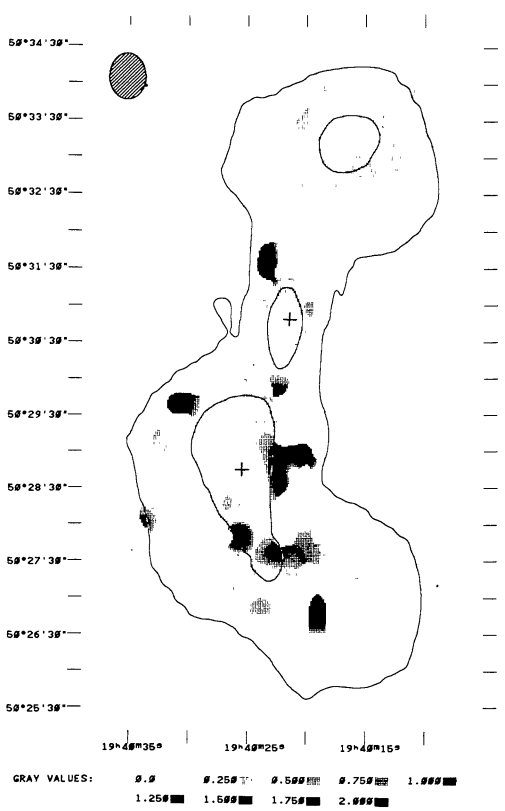

FIGURE 11h. — The distribution of the depolarization of 3C402 between 0.6 GHz and 1.4 GHz. The two levels in the total intensity contour map at 0.6 GHz are 8 and 192 mJy/beam.

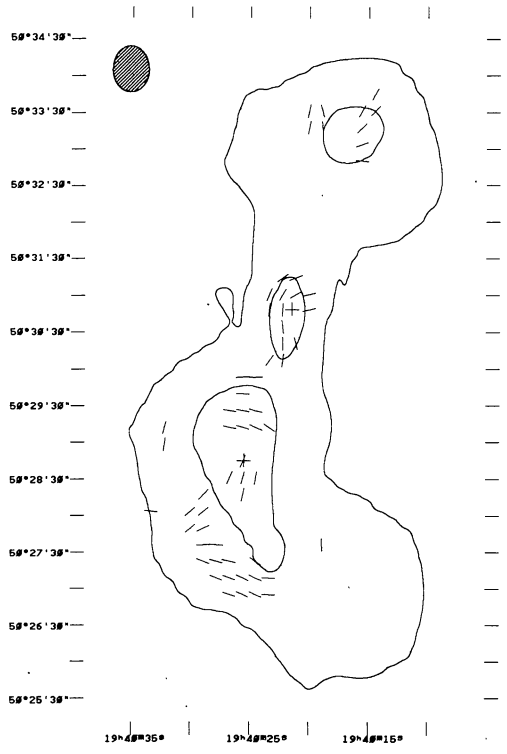

FIGURE 11i. — The distribution of the rotation of the polarization position angle of 3C402 between 0.6 GHz and 1.4 GHz measured from the North towards the East. The two levels in the total intensity contour map at 0.6 GHz are 8 and 192 mJy/beam.

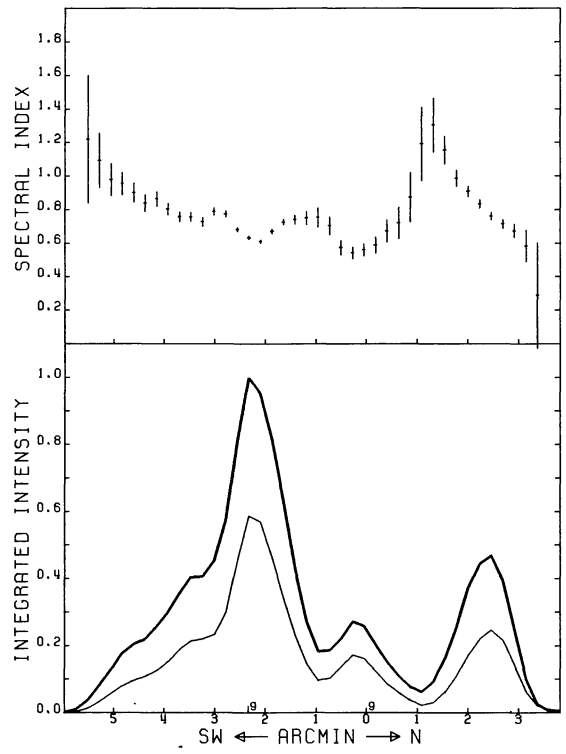

FIGURE 11j. — The spectral index variations along the major axis of 3C402 between 0.6 GHz and 1.4 GHz. The lower panel shows the (integrated) total intensity along the radio source at 0.6 GHz (thick line) and at 1.4 GHz (thin line). The upper panel shows the variations of the spectral index along the radio source.

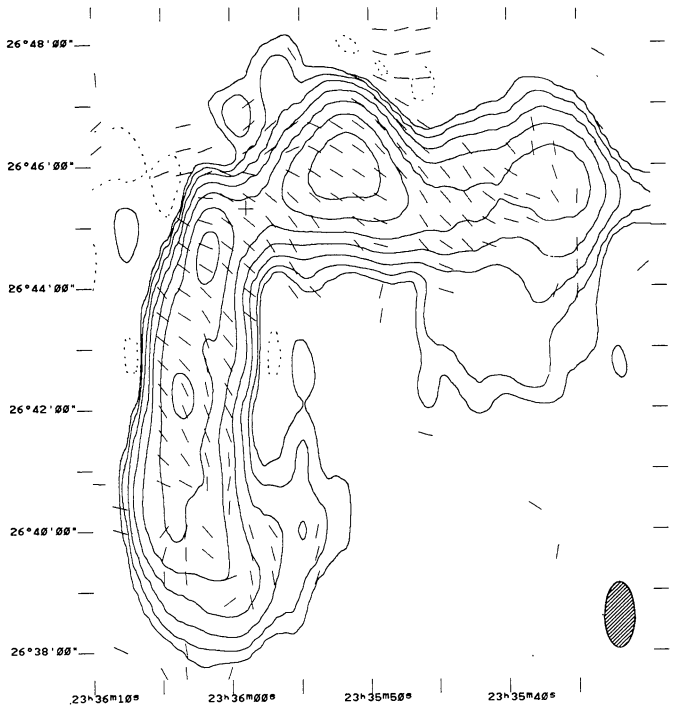

FIGURE 12a. — The total intensity distribution of 3C465 at 0.6 GHz. The contour levels are – 15, 15, 30, 60, 120, 240, 480 and 960 mJy/beam.

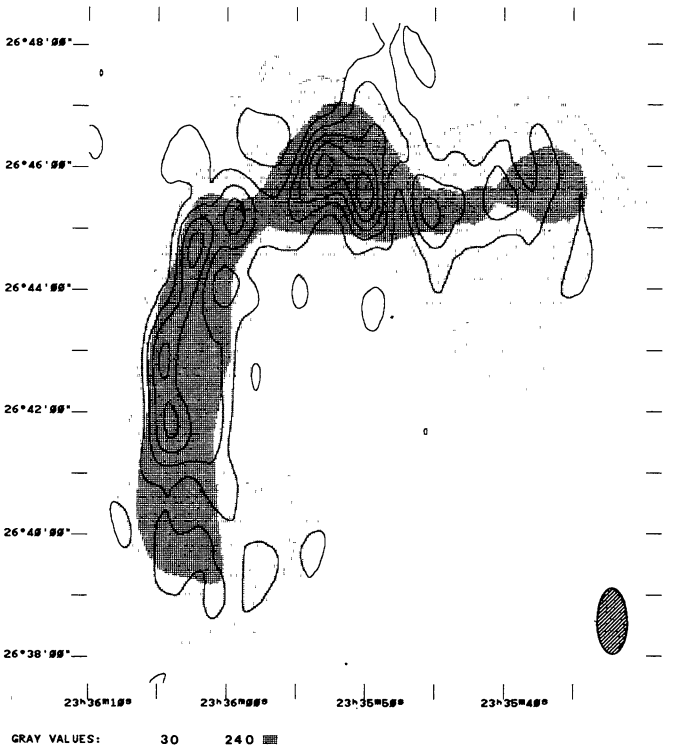

FIGURE 12b. — The linearly polarized intensity distribution of 3C465 at 0.6 GHz. The contour levels are 1.5, 3, 4.5, 6 and 7.5 mJy/beam.

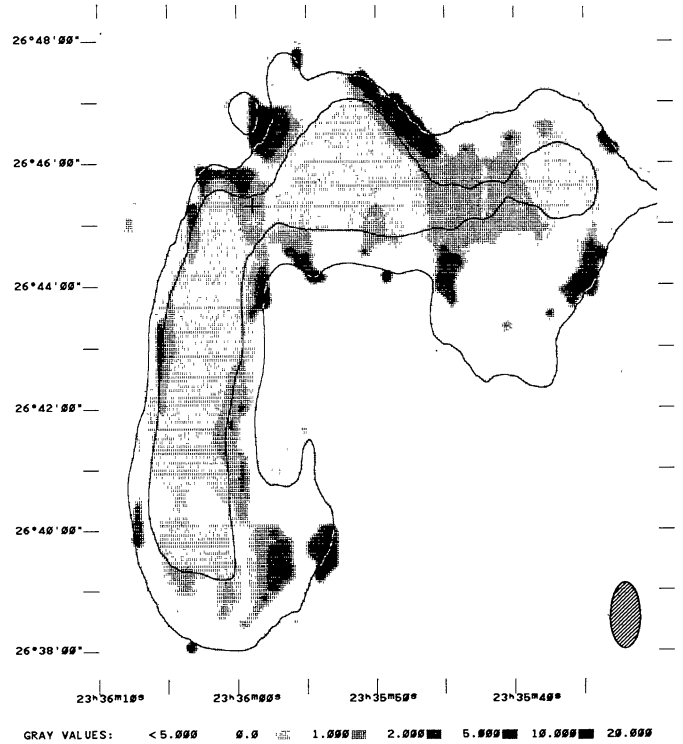

FIGURE 12c. — The distribution of 3C465 at 0.6 GHz. The two levels in the total intensity contour map are 30 and 240 mJy/beam.

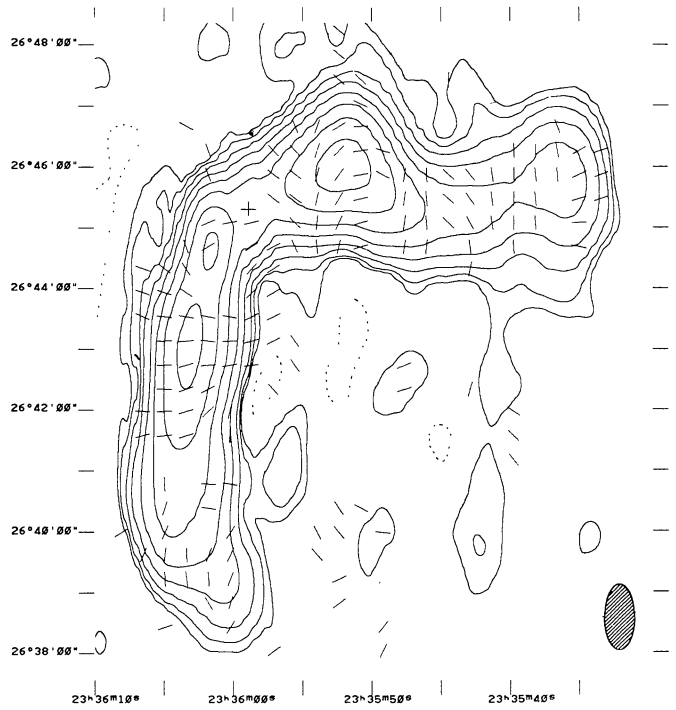

FIGURE 12d. — The total intensity distribution of 3C465 at 1.4 GHz. The contour levels are – 10, 5, 10, 20, 40, 80, 160, 320 and 640 mJy/beam.

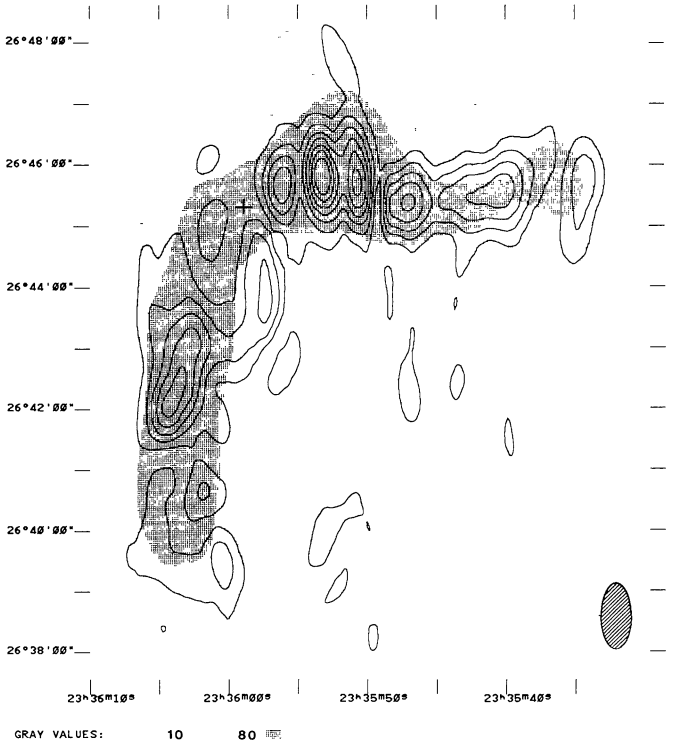

FIGURE 12e. — The linearly polarized intensity distribution of 3C465 at 1.4 GHz. The contour levels are 4, 8, 12, 16, 20, 24 and 28 mJy/beam.

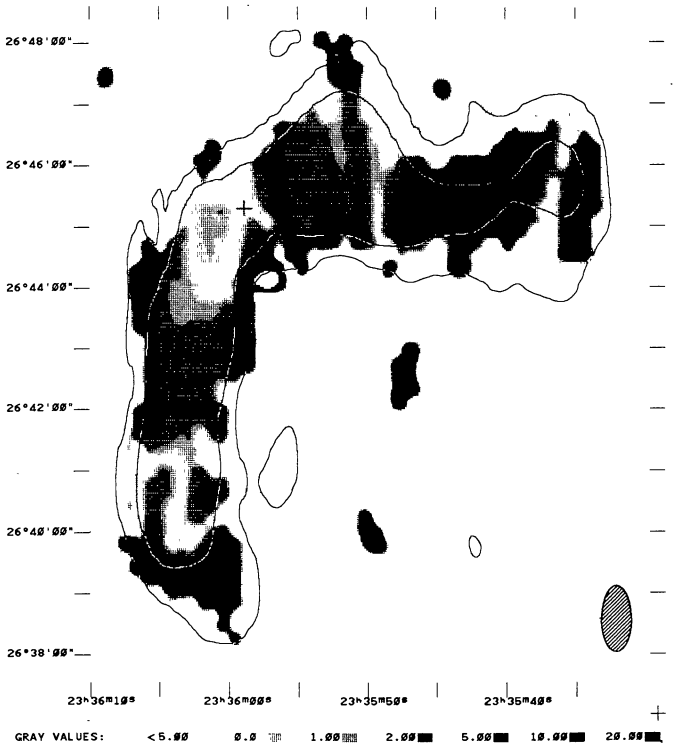

FIGURE 12f. — The distribution of the percentage polarization of 3C465 at 1.4 GHz. The two levels in the total intensity contour map are 10 and 80 mJy/beam.

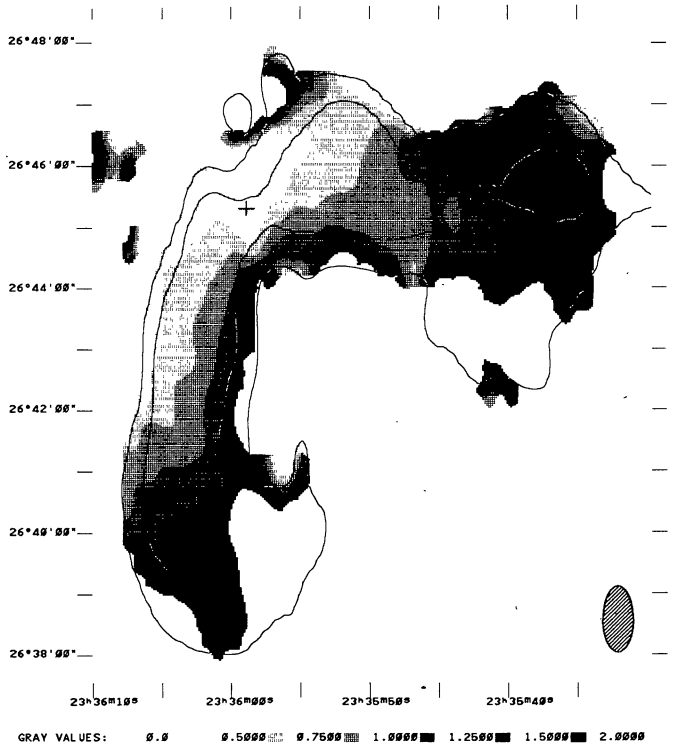

FIGURE 12g. — The distribution of the spectral index of 3C465 between 0.6 GHz and 1.4 GHz. The two levels in the total intensity contour map at 0.6 GHz are 30 and 240 mJy/beam.

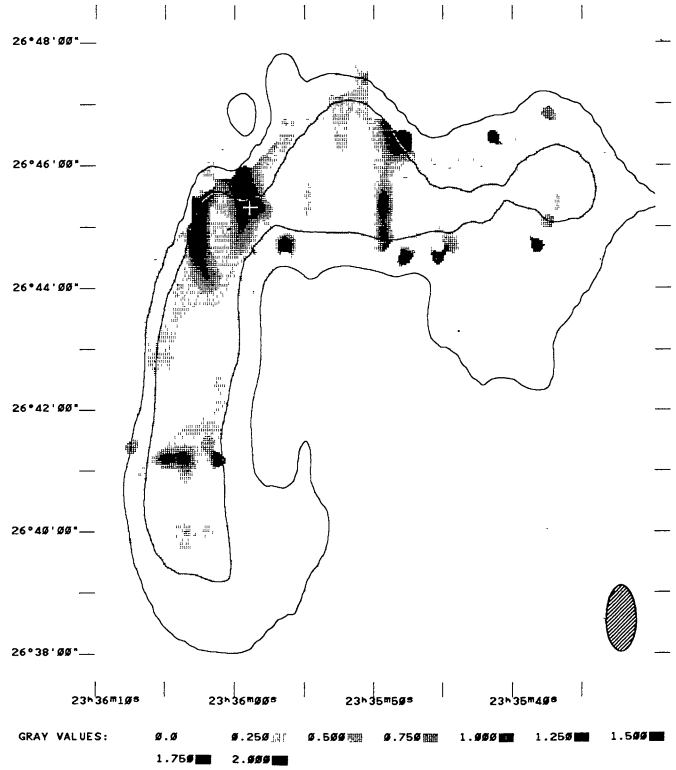

FIGURE 12h. — The distribution of the depolarization of 3C465 between 0.6 GHz and 1.4 GHz. The two levels in the total intensity contour map at 0.6 GHz are 30 and 240 mJy/beam.

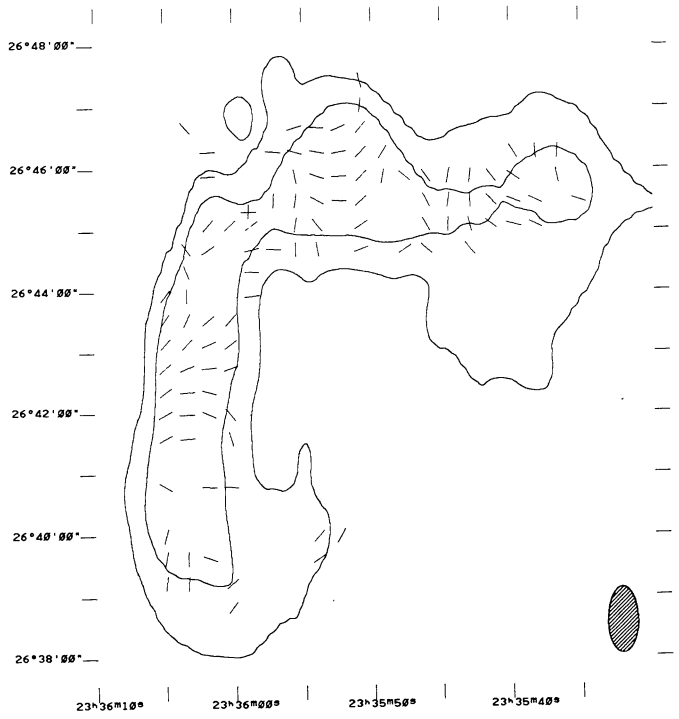

FIGURE 12i. — The distribution of the rotation of the polarization position angle of 3C465 between 0.6 GHz and 1.4 GHz measured from the North towards the East. The two levels in the total intensity contour map at 0.6 GHz are 30 and 240 mJy/beam.

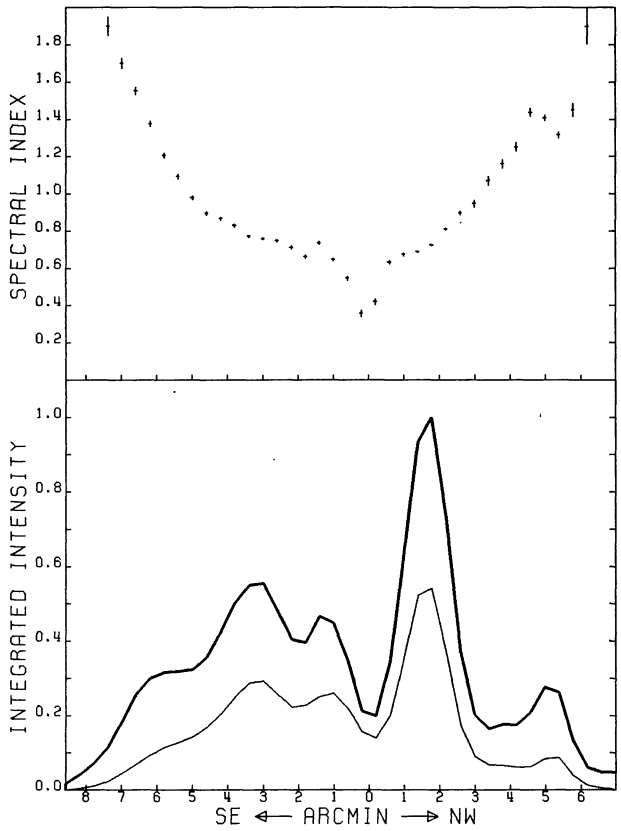

FIGURE 12j. — The spectral index variations along the major axis of 3C465 between 0.6 GHz and 1.4 GHz. The lower panel shows the (integrated) total intensity along the radio source at 0.6 GHz (thick line) and at 1.4 GHz (thin line). The upper panel shows the variations of the spectral index along the radio source.